RESEARCH

Probing the multitargeting potential of *n*-hexane fraction of *Gongronema latifolium* leaves in neurodegeneration via in vitro, GC–MS and in silico studies

Gideon A. Gyebi[1,2]* , Joseph C. Ejoh[1], Oludare M. Ogunyemi[3], Auza Moses Ibrahim[4], Ibrahim M. Ibrahim[5], Saheed O. Afolabi[6], Gabriel O. Anyanwu[1], Rotimi J. Ojo[7], Olalekan B. Ogunro[8], Badriyah S. Alotaibi[9] and Gaber El-Saber Batiha[10]

Abstract

Background Neurodegenerative disorders (NDDs) are associated with increased activities of brain acetylcholinesterase (AChE), butyrylcholinesterase (BChE) and monoamine oxidase (MAO) as well as Aβ-amyloid (Aβ) neurotoxicity; therefore, they offer a therapeutic option for the treatment of NDDs such as Alzheimer's disease (AD). This study was aimed at identifying multi-targeting neurotherapeutics from *Gongronema latifolium* leaves using in vitro analysis, GC–MS profiling and computational methods.

Results The *n*-hexane solvent partition fraction of the methanol extract of *Gongronema latifolium* leaf (HF) exhibited concentration-dependent inhibitory activities against acetylcholinesterase and butyrylcholinesterase but not against MOA in vitro. The GC–MS chemical profiling identified 17 phytochemicals from the HF; these were further screened against human AChE, BChE, β-secretase enzyme (BACE1) and amyloid-β (Aβ) fibrils using molecular docking, ensemble-based docking (EBD), molecular dynamics simulation (MDs) and binding free energy (BFG) coupled with predictive adsorption, distribution, metabolism, excretion and toxicity (ADMET) analysis. The lead phytochemicals (LPs) (dihydroactinidiolide and 1H-Indole-3-ethanamine), with mean binding energies (-6.525 ± 0.895 and 6.475 ± 0.985; -6.833 ± 0.461 and -6.466 ± 0.577; -6.2 ± 0.845 and -5.95 ± 0.353 kcal/mol) exhibited multi-target binding tendencies to the catalytic residues of hAChE, hBChE and hBACE1, in addition to hAβ fibril-disruptive tendencies (-6.325 ± 0.545 and -5.95 ± 0.353 kcal/mol), respectively. These results corroborated the initial molecular docking and BFG computations. The lead phytochemical–protein complexes were stable during the period of MDs. The LP presented favorable drug-likeness and ADMET properties coupled with the capacity to traverse the BBB.

Conclusion Dihydroactinidiolide and 1H-Indole-3-ethanamine, in part or in synergy, are identified as neurotherapeutic constituents of *Gongronema latifolium* that may have been responsible for the ethnopharmacologically reported neurotherapeutic activities of the leaf, and hence they are suggested as potential drug candidates that can be useful for managing or treating neurodegenerative disease such as Alzheimer's disease, subject to further investigation.

Keywords *Gongronema latifolium*, Acetylcholinesterase, Butyrylcholinesterase, Monoamine oxidase, Amyloid-β (Aβ) fibrils, Ensembled-molecular docking, dihydroactinidiolide, 1H-Indole-3-ethanamine

*Correspondence:
Gideon A. Gyebi
gideonagyebi@gmail.com
Full list of author information is available at the end of the article

Background

Neurodegenerative disorders (NDDs) are a cluster of ailments with features of progressive degeneration of the function and structure of human nervous tissues, causing deterioration in brain performance and ultimately leading to death. Besides, they cause a decrease in the quality of life of the patients. Huntington's disease, Alzheimer's disease (AD), Parkinson's disease (PD), and dementia are among the most pressing NDDs of global concern, especially among geriatrics [1]. Throughout sub-Saharan Africa, AD and other NDDs have been projected to increase the burden on health systems; to the same extent, over half of dementia patients are situated in low- and intermediate-income countries such as Nigeri [2, 3]. The incidence of age-adjusted dementia in the sub-Saharan part of Africa has been estimated by Alzheimer's Disease International to be 7.2% among those that are 60 years of age and older [2]. Globally, approximately 5.4 and 10 million people are suffering from AD and PD, respectively [4], revealing that NDDs are among the foremost causes of death [1, 5]. Current studies predict a universal upsurge in the incidence of dementia cases from 57.4 million in 2019 to a range of (130.8–175.9) million in 2050 [6]. Marking multiple causes of NDDs is a modern approach for the development of prospective therapeutics for NDDs. Such pathological processes involved in neuronal degeneration may include decline in brain neurotransmitters, oxidative stress, inflammation, mitochondrial dysfunction, apoptosis, genetic factors and misfolding of proteins that tend to aggregate, accounting for their multiple aetiologies [7]. In the brain, one of the pathological changes that is associated with NDDs involves a decline in neurotransmitters, including neuroactive amines, acetylcholine and butyrylcholine. Specifically, AD has the distinctive characteristic of deficient acetylcholine; consequently, several therapeutic possibilities involve the enhancement of cholinergic transmission [8].

Cholinergic neurons use acetyl- and butyrylcholine for neurotransmission; after their release to the synaptic cleft, the cholinesterases hydrolyze acetyl- and butyrylcholine into acetate and choline [9]. The increased activities of these enzymes may lead to cholinergic insufficiency and a decline in intellectual ability; therefore, there is a need for compounds that can serve as cholinesterase inhibitors. Such inhibition strategies will raise the intensity of acetylcholine and butyrylcholine in the synaptic cleft and thus improve interactions and transmission between neurons in the brain. In this direction, several inhibitors of cholinesterase have been designed as therapeutics for NDDs management [10]. These cholinesterase antagonists are also used to treat NDDs, which are characterized by degeneration in cholinergic conduction, including dementia and Lewy bodies [11]. The deficit of dopamine in the substantial nigra pars compacta and dopaminergic neurons is the hallmark of PD [12]. Also, inhibitors of enzymes such as monoamine oxidase (MAO), known to catalyze the oxidative deamination of dopamine, will relieve some of the indicators associated with PD and other NDDs [1]. In this regard, several studies that employ the cholinergic and MOA enzymes as drug targets have produced clinically approved inhibitors, but not without side effects. Furthermore, the buildup of proteins that are misfolded is a common factor implicated in the aetiology of AD and PD, whose aggregation leads to the stultification of synaptic function and the deadening of neurons [13]. The plaques produced from extracellular β-amyloid coupled with intracellular neurofibrillary tangles that are formed as a result of the excessive phosphorylation of the tau protein are the main contributors to the pathophysiology of Alzheimer's disease [1]. The β-secretase enzyme (BACE1), which is also called the β-site amyloid progenitor protein (APP) splitting enzyme 1, is an aspartic protease found in the transmembrane, whose main function is the cleaving of the transmembrane amyloid protein to produce the β-stubs and is implicated as a rate-limiting catalytic step that produces Aβ [14]. It is therefore conceivable that inhibitors of BACE1 enzymes may afford curative and remedial alternatives for the management and remedy of Alzheimer's disease. The protein concentration and enzyme activity of this protein in the body fluids of humans are promising candidate biomarkers, which have also been exploited toward the development of inhibitors that may delay or arrest the imbalance of the amyloid-β pathway in Alzheimer's disease [14, 15]. In addition, several reports have implicated oxidative stress, which may induce the accumulation of metal ions in the brain [7]. Oxidative stress observed in patients with NDDs has been linked to the accumulation of iron in their brains [16]. Although iron is an important element with key physiological functions, such as components of proteins and cofactors, excessive free iron may produce oxidative stress conditions, especially in the brain, with relatively diminished anti-oxidative defense. Ferrous iron, through the Fenton reaction, can stimulate oxygen toxicity, which may cause the generation of free radicals, including hydroxyl radicals (·OH), that will ultimately result in oxidative stress. The development of oxidative stress implies either an overwhelming of the antioxidant defense mechanisms or excessive free radicals or oxidant species. As suggested earlier, compounds with metal chelating and antioxidant activities may play a vital role in neuroprotection [17, 18]. Aiming at

numerous causative players in neurodegenerative disorders is a modern approach for the enhancement and promotion of prospective intervention for NDDs.

Numerous food herbs and therapeutic plants are known for their neuroshielding and antioxidant performance, as they have been conventionally used for the management of Alzheimer's disease and other NDDs. These plants include: *Crocus sativus* L. (saffron) [19], *Nigella sativa* L. [20], *Coriandrum sativum* [21], *Ferula assafoetida* [22], *Thymus vulgaris* [23], *Zataria multiflora* Linn [24]*, Curcuma longa* Linn [22] and *Gongronema latifolium* Benth [25]. Rapid in vitro and in silico techniques are valuable for deciphering the interactions of the bioactive constituents of such plants and selected targets in diseases toward the identification of preventive nutraceuticals and therapeutic agents. In particular, computational methods such as molecular docking, molecular dynamics simulation and quantitative structure–activity relationships (QSARs) have been effectively employed to predict bioactive components from food herbs and medicinal plants [26, 27]. Several anti-Alzheimer's agents have been suggested through such in silico computational analysis of natural compounds [28].

Gongronema latifolium, a green leafy vegetable widely consumed in Nigeria and some African regions, has been widely reported for its neuroprotective and antioxidant properties [29–31]. Although previous studies, which include computational screening, have suggested the polypharmacology potential of GL in NDDs [28, 30], there is a paucity of information on the in vitro testing of the bioactive fractions and isolates. Integrating in vitro testing with computational studies may provide further empirical evidence for the ethnopharmacological use of this plant. Therefore, the current study employs in vitro, GC–MS chemical profiling and various in silico methods to investigate the inhibitory capacity of the *n*-hexane solvent fraction of the methanol extract of *Gongronema latifolium*.

Methods
Plant material
Gongronema latifolia leaves were authenticated with a voucher number that was deposited.

Extraction and preparation of n-hexane extract
The method described by [32] was used for the extraction of the 80% methanol extracts. The methods used for the extraction, solvent–solvent partitioning of the *n*-hexane extract have been reported in our previous study Gyebi et al. [33]. Briefly, 10 kg of *G. latifolium* leaves (UILH/002/1176) was air-dried to a uniform weight of 2.2 kg; this was further macerated in 80% methanol (12 L of methanol and 2.4 L of distilled water) for two weeks at room temperature. Using a rotary evaporator, the solvent was removed under reduced pressure with a total yield of methanol extract (180 g). The extracts were further successively partitioned with *n*-hexane (3 L) and EtOAc (3 L) in this order, giving rise to 3 fractions: *n*-hexane (40 g), EtOAc (62 g) and residue (78 g).

In vitro analysis
Determination of cholinesterase inhibitory activities
The inhibitory activities of the *n*-hexane fraction of *Gongronema latifolia* extract on acetylcholinesterase and butyrylcholinesterase were assessed using spectrophotometric method based on Ellman method [34] as modified [35]. Acetylcholine iodide ($C_7H_{16}NO_2I$) and butyrylcholine iodide ($C_9H_{20}INO_2$) were used as substrates and final concentrations of 50, 100, 150, 200 and 250 μg/mL of the extract. A mixture of 500 μL of phosphate buffer (PH 8.0, 0.1 M), 200 μL of acetylcholinesterase enzyme solution, 100 μL solution of 3.3 mM 5,5-dithio-bis (2-nitrobenzoic) acid and various intensities of the test samples, were pipetted into the microplates. In total, 100 μL of acetylthiocholine iodide (0.05 mM) was added after the mixture was incubated for 20 min at 25 °C. The acetylcholinesterase activity that occurred within 3 min at room temperature was measured at an absorbance of 412 nm.

Using the substrate butyrylthiocholine, the same procedure was employed to measure butyrylcholinesterase activity [35]. The obstructive activity of the enzyme was computed and presented as percentage inhibition. Methanol was used as the negative control. While the assay was carried out in duplicates

$$\text{Inhibition\%} = [(\text{Abs}_{cont} - \text{Ab}_{sam})/\text{Abs}_{cont}] \times 100$$
$$(1)$$

where Abs_{cont} is the change in absorbance of the negative control, and Ab_{sam} is the change in absorbance of the sample.

Determination of monoamine oxidase inhibitory activities
The MOA inhibitory action of the *n*-hexane partition fraction of *Gongronema latifolia* determined based on earlier stated method [36]. The reaction combination consists of phosphate buffer (0.025 M at pH 7), semicarbazide (12.5 mM), benzylamine (10 mM at pH 7), 75 μL of enzyme (MAO) and 250, 200, 150, 100 and 50 μg/mL solution of water-dissolved test samples. Acetic acid (250 μL) was included after 30 min and boiled for 3 min in water bath after that the mixture was centrifuged. The resultant supernatant (1 mL), 0.05% of 2, 4-DNPH (1.25 mL) and 1.25 mL benzene were mixed prior to the incubation at rt for 10 min. Equal volumes of sodium hydroxide (1 N) and isolated benzene layer of the mixture above were mixed and heated for 10 min at 80 °C. The

Gyebi *et al. Future Journal of Pharmaceutical Sciences*   (2023) 9:84

Page 4 of 33

alkaline layer was poured out [37]. The alkaline layer was decanted [37]. The absorbance was measured at a wavelength of 450 nm. The inhibition in percentage was determined as follows: The assay was run in 3 replicates.

$$[(\text{Abs}_{\text{Control}} - \text{Abs}_{\text{Samples}})/\text{Abs}_{\text{Control}}] \times 100 \qquad (2)$$

Statistical analysis

One-way ANOVA and Duncan multiple range were used to measure for statistical difference among the means of the concentrations in IBM SPSS Statistics version 23.0 (IBM Corp., Armonk, N.Y., USA). Difference at $p < 0.05$ was considered significant. Graphs were created using Microsoft excel for windows 2016.

GC–MS identification of chemical constituent of *n*-hexane fraction of the methanol fraction of *Gongronema latifolium* leaf extract

The GC–MS investigation of the *n*-hexane fraction of the methanol fraction of *Gongronema latifolium* leaf extract was executed on automatic sampler system (Agilent 19091GC plus) that is paired with a quadruple Mass Spectrometer 433HP-5MS. The test sample was infused at about 250 °C with a split ratio of 10:1 with a flow rate of helium 1 mL/min. The phytocompounds were then removed in HP5MS column merged with phenylmethylsilox (length; 30 m×250 µm; film thickness 0.25 µm). The carrier gas used was helium operated at a flow rate of 1 mL per minute. GC-FID detector was used to detect the phytocompounds; each signal was fragmented on the mass spectrometry for compound identification. The chromatogram is presented as Fig. 2.

In silico studies

Retrieval and preparation of proteins

The co-crystallized proteins of *human* acetylcholinesterase (hAChE) with donepezil (4EY7), *human* butyrylcholinesterase (*h*BChE) with propidium (6ESJ) *human* β-secretase (BACE-1) with aminoquinoline compound 1 (5I3V) and unbound Aβ fibrils (2BEG) were saved from the http://www.rcsb.org (Protein Data Bank website). The water and co-crystallized ligand molecules accompanying the protein make up were deleted, while lost hydrogen atoms were added using MGL-AutoDockTools (ADT, v1.5.6). The Kollman charges were inserted as the partial atomic charge [38].

Ligands preparation

The Structure Data Format (SDF) of the GC–MS identified phytocompounds from the *n*-hexane fraction of *Gongronema latifolium* Benth Leaf and the co-crystalized compounds (donepezil and propidium) were assessed from the PubChem database (www.pubchem.ncbi.nlm.

nih.gov), while compound 1 the native ligand for 5I3V was extracted from the crystal structure. The compounds were minimized using in OpenBabel [39]. The AutoDock function tools as implemented in PyRx 0.8 were used to convert the ligands to PDBQT format [40].

Molecular docking studies

Active site directed and blind molecular docking of phytochemicals to target proteins

The procedure for the molecular docking analysis was validated before the docking of the compounds to the proteins. The GC–MS identified compounds and the reference inhibitors (donepezil, propidium an aminoquinoline compound) were docked to the active site of *h*AChE and *h*BChE and *h*BACE-1 using AutoDock Vina in PyRx 0.8 [40]. The ligands were decreased after importation with OpenBabel in PyRx 0.8 [39]. For the optimization algorithms, the conjugate slope descent was utilized, while for energy minimization parameter, the Universal Force Field (UFF) was employed. The dimension of the binding site of the enzymes was characterized by the grid box size, and center is presented in Table 1. In all the docking processes, default mode was implemented. The active site directed docking was executed for proteins which know active site (hAChE, bAChE and BACE-1), the amino acid regions around the native ligands were selected, and the grid box was drawn around them, while the grid box enveloped the whole surface of the proteins for the blind docking analysis for the Aβ fibrils.

Molecular dynamics

Two different MD simulation analyses were undertaken using the same protocol in this study. In the first analysis, the native ligand for the proteins was extracted, after which the apo proteins were exposed to a full-atomistic 100-ns simulation. The trajectories obtained from this analysis were clustered for the optimized docking study. In the second analysis, the reference compounds and the 2 lead phytochemicals complexed with the proteins were subjected to 100-ns simulation

Table 1 Targets protein binding coordinates

Dimensions	Aβ fibrils (Å)	BACE-1 (Å)	hAChE (Å)	bAChE (Å)
Center_x	0.55	67.91	− 13.48	2.54
Center_y	0.02	48.43	− 43.40	− 9.30
Center_z	− 8.25	9.57	27.61	− 14.86
Size x	52.76	16.72	24.78	18.53
Size y	22.91	16.24	16.73	21.94
Size z	32.81	19.95	19.87	17.05

Blind docking of the ligands was performed against Aβ fibrils, while targeted docking was performed against BACE-1, hAChE and hBChE

Gyebi *et al. Future Journal of Pharmaceutical Sciences*   (2023) 9:84

Page 5 of 33

for firmness and conformation analysis of the bound complexes. In both case, the molecular dynamic (MD) simulation was performed using GROMACS 2019.2 and GROMOS96 43a1 forcefield [41–43]. The ligands topology files were generated using PRODRG webserver (http://davapc1.bioch.dundee.ac.uk/cgi-bin/prodrg) [44]. The systems of the apo enzymes and the ligand–bound enzymes complex were all solvated with transmittable intermolecular potential with a fourpoint (TIP4P) within a cubic box water model, with periodic limit conditions applied at a physiological concentration of 0.154 M set by neutralized NaCl ions. The systems were minimized for 10,000 steps using steepest descent algorithm in constant number of atoms, volume and temperature ensemble (NVT) ensemble for 0.3 ns, followed by 0.3 ns of equilibration in constant number of atoms, constant pressure and constant temperature (NPT). The pressure and temperature were set to 1 atm and 310 K and sustained using Parrinello-Rahmanbarostat and velocity rescale, respectively. Leap-frog integrator was used with a time step of 2 femtosecond. Fifty nanoseconds of simulation was performed for each system, and for each 0.1 nano a snapshot was saved giving rise to a total of 1000 frames. The VMD TK console scripts [45] were used to analyze the lines produced from the simulation to calculate RMSD, RMSF, SASA, RoG and number of H-bond.

Clustering of molecular dynamic trajectories of unbound proteins

In preparation for an ensemble docking analysis, TTClust V 4.9.0 [46] was employed for the clustering of the trajectories acquired from MD simulation of the apo proteins. The trajectories were clustered using TTClust python package that employs the elbow method to determine the optimal number of clusters from which representative frame for each of the cluster is provided. This representative conformation for each cluster was used in the optimized docking experiment.

Ensembled-based docking of the GC–MS identified phytocompounds to various conformations of the proteins

The GC–MS identified phytochemicals and the reference compounds were docked to the actives sites of the selected representative structure of target proteins that were acquired from the cluster analysis of the MDS trajectories using AutoDock Vina software [38, 40]. The Universal Force Field (UFF) was employed in the optimization using the steepest descent algorithm [47–49]. The selected docked conformation was analyzed using Discovery studio visualizer [50].

Binding free energy calculation using MM-GBSA

The gmx_MMPBSA package was used to compute the free energy of binding using Molecular Mechanics Generalized Born Surface Area (MM-GBSA) algorithm for each enzyme_lead phytochemical complex systems. The binding energies were decomposed to get the amino acids within 10 Å around the ligand [51, 52]. The strength of salt and solvation (igb) were set to 0.154 M and 5, respectively, while the external and internal dielectric constants were set to 78.5 and 1.0, respectively. Other parameters were set as default.

$$\Delta G = G_{\text{complex}} - G_{\text{receptor}} - G_{\text{ligand}} \qquad (3)$$

Different energy terms were estimated according to Eqs. 2–6>

$$\Delta G_{\text{binding}} = \Delta H - T\Delta S \qquad (4)$$

$$\Delta H = \Delta E_{\text{gas}} + \Delta E_{\text{sol}} \qquad (5)$$

$$\Delta E_{\text{gas}} = \Delta E_{\text{ele}} + \Delta E_{\text{vdW}} \qquad (6)$$

$$\Delta E_{\text{solv}} = E_{\text{GB}} + E_{\text{SA}} \qquad (7)$$

$$E_{\text{SA}} = \gamma \cdot \text{SASA} \qquad (8)$$

where ΔH is the calculated enthalpy from solvation-free energy (E_{sol}) and gas-phase energy (E_{gas}). So as to match the relative binding free energies, the $T\Delta S$ which represents entropic donation to the free binding energy was not estimated in this study. E comprises of van der Waals (E_{vdW}) and electrostatic (E_{ele}) terms. E_{sol} was computed from the polar solvation energy (E_{GB}), while (E_{SA}) nonpolar solvation energy was assessed from the accessible solvent surface area [53, 54]

Results

In vitro studies

Cholinesterase and monoamine oxidase inhibitory activities

AChE and BchE activity assay plays an imperative role in vitro characterization and identification of potent inhibitors of the enzymes that serve as drugs for potential treatments for AD [55]. The inhibitory activities of the solvent-partitioned *n*-hexane fraction of the MeOH extract of *Gl* on acetylcholinesterase and butyrylcholinesterase and monoamine oxidase actions were investigated using in vitro inhibition assays. For AChE and BChE activities a concentration-dependent (CD) inhibitory activities were recorded by HF of *Gl*, while HF of *Gl* did not show a CD inhibition of monoamine oxidase activity (Fig. 1).
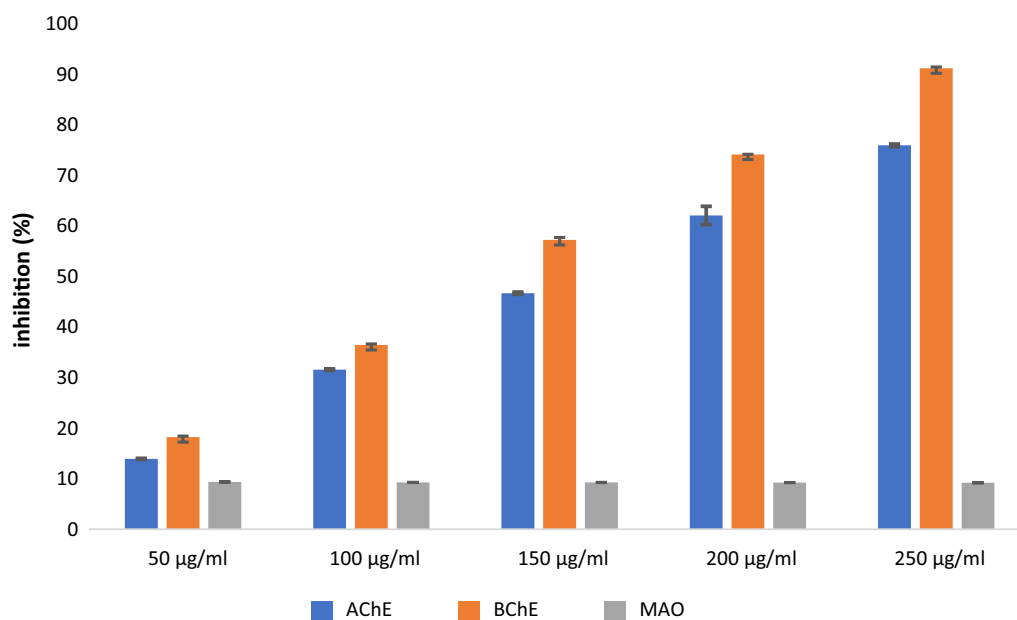
Fig. 1 Inhibitory activities of *n*-hexane partition fraction of the MeOH extract of *Gl* against AChE, BChE and MOA (*n* = 3)

GC–MS identification of chemical constituent

The GC–MS chromatogram of the *n*-hexane fraction of methanol extract of *Gongronema latifolium* leaves extract (Fig. 2), shows the peaks of the compounds identified in the fraction. The identified phytocompounds were based on retention time, the peak area and molecular formula. Table 2 shows the name of the phytocompounds, retention time (RT) its molecular formula and percentage peak area. The sum of 17 compounds was identified. Cambamic acid and 1,3-dimethyldiaziridine with close RT of 3.726 and 3.876 were identified to have the high percentage area, signifying the richness of the compound in the fraction.

In silico analysis

Authentication of molecular docking protocol

Authentication of molecular docking procedure is an import step in virtual screening of compounds that is applied to the protocol to predict the precision and accuracy of the docking protocol [56]. An initial validation of the docking procedure to be used for the docking steps was undertaken. The extracted co-crystalized ligands (propidium, donepezil, and aminoquinoline compound of *h*BChE *h*AChE and *h*BACE1 were superimposed, respectively) were superimposed and aligned on the selected docked poses with the least energetic conformer. The RMSD calculated on BIOVIA Discovery Studio Visualizer 20.1.0, San Diego, CA, USA, 2020 was 0.6005, 0.5761 and 0.000 Å for propidium,

donepezil, and aminoquinoline compound, respectively (Fig. 3).

Molecular docking study

The results of the molecular docking of the GC–MS identified phytochemicals (17) (GIP) and reference compounds (donepezil, propidium and aminoquinoline compound 1) against *h*AChE, *h*BChE and *h*BACE-1 are presented in (Table 1). The ranges of binding energies are (−8.0 to −3.4; −7.7 to −2.8; −7.1 to −3.1 and −9.1 to 6.5 kcal/mol for *h*AChE, *h*BChE, *h*BACE1 and *h*Aβ fibrils), respectively. The binding energies for the reference compounds (donepezil, propidium and aminoquinoline compound 1) for the *h*AChE, *h*BChE and *h*BACE1 enzymes are −12.2, −9.3 and −7.7 kcal/mol, respectively. Based on the binding scores, docked poses and interaction with the catalytic residues of the respective proteins, the top two phytochemicals were selected and the lead phytochemicals to the proteins. Dihydroactinidiolide was the top lead phytochemicals to the four proteins with a binding energies of −8, −7.1, −7.7 and −9.1 kcal/mol for *h*AChE, *h*BChE, *h*BACE1 and *h*Aβ fibrils, while 1H-Indole-3-ethanamine had the second best binding energies of −6.7, −6.8 and −8.9 kcal/mol for *h*BChE, *h*BACE1 and *h*Aβ fibrils proteins. Thymol (−7.5 kcal/mol) was the second lead phytochemical for the *h*AChE enzymes. Therefore, dihydroactinidiolide and 1H-Indole-3-ethanamine exhibited multiple high binding tendencies to atleast 3 of the protein target. Thymol was
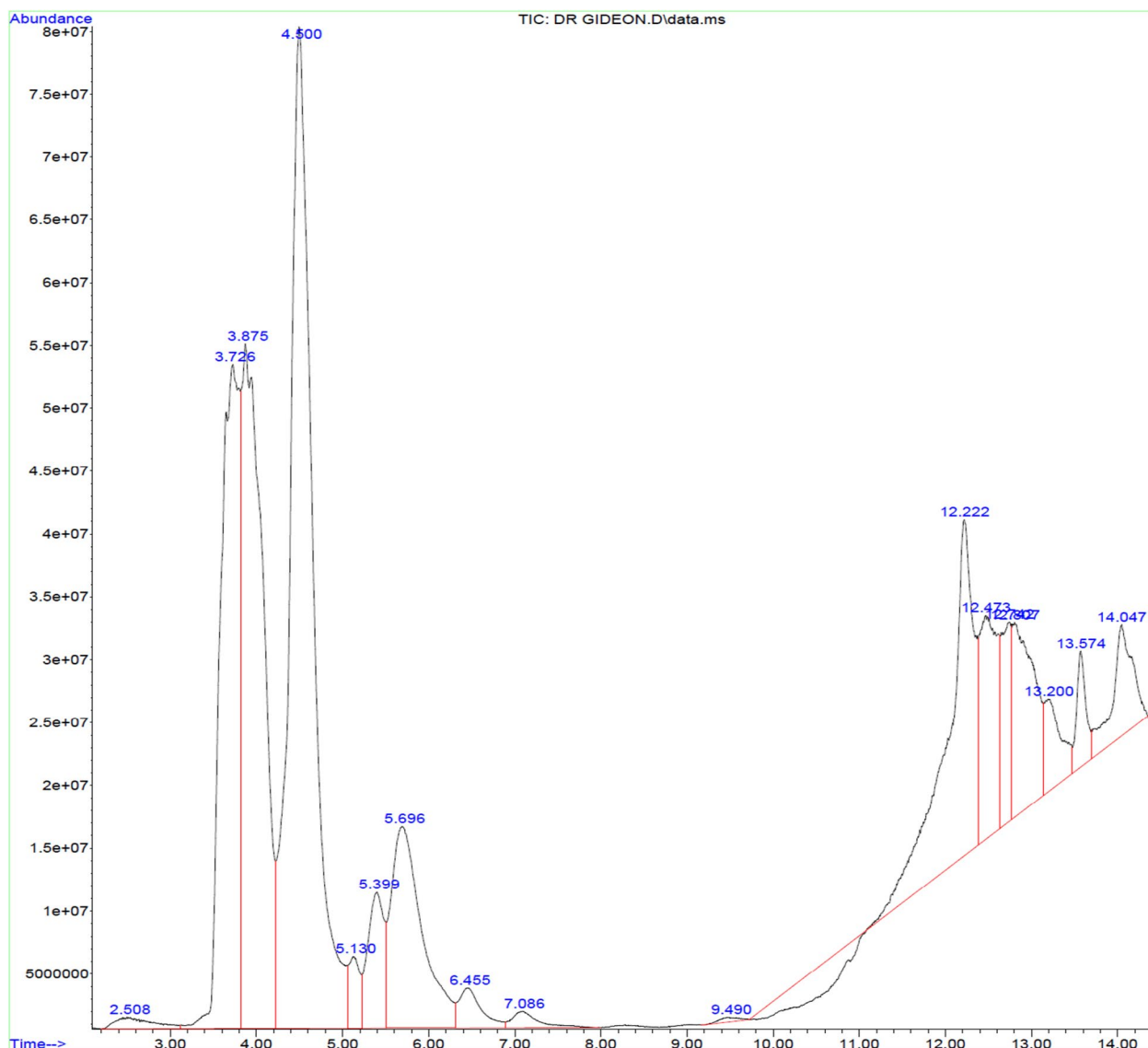
Fig. 2 Chromatogram of phytocompounds in *n*-hexane fraction of 80% methanol *Gongronema latifolium*

also ranked among the best 5th phytochemicals to the 3 other proteins targets (Table 3).

Amino acid interactions of the lead phytochemicals with the residues of human acetylcholinesterase, human butyrylcholinesterase, human β-secretase and hAβ fibrils
Table 4 reveals the numerous binding interactions in the active groove of the proteins. The interactive analysis shows that donepezil, the co-crystalized ligand of hAChE, was docked in the active gorge of the enzyme. The 1-benzyl unit of donepezil made aromatic Pi-Pi stacking to His447 and Trp86. Two Pi-alkyl interactions with Tyr337 and Tyr341 were observed with the piperidine ring. The 5-methoxy unit of inden-1-one and the piperidine

ring formed two Pi-sigma interactions with Trp286 and Phe338, respectively. The only hydrogen bond that was recorded in the interaction was between Phe295 and the carbonyl oxygen of the indenone ring (Fig. 4). The bond between dihydroactinidiolide and hAChE was stabilized by an H-bond amid the carbonyl oxygen of the benzo-furan-2-one ring and Gly122. Phe333 made four hydro-phobic interactions that included 3 Pi-alkyl contacts with the three methyl groups and an additional Pi-sigma bond to 4-methyl group of dihydroactinidiolide. Tyr341 made 2 Pi-alkyl contacts with 4 and 4a methyl groups, while Try337 formed a sigma interaction with a 7-methyl group and 2 Pi-alkyl contacts with 4 and 4a methyl groups. The interactions between thymol and hAChE were stabilized

Gyebi *et al. Future Journal of Pharmaceutical Sciences*   (2023) 9:84

Page 8 of 33

Table 2 Identified compounds in the *n*-hexane fraction of 80% methanol extract *Gongronema latifolium*

S no.	Name of phytocompound	RT	Formulae	Molecular mass (g/mol)	Area %
1	2,5-Dihydro-5-methoxy-2-furanone	2.506	$C_5H_6O_3$	114.1	0.52
2	Carbamic acid	3.726	CH_3NO_2	61.04	14.65
3	1,3-Dimethyldiaziridine	3.876	$C_3H_8N_2$	72.11	17.94
4	1-Octanol, 3,7-dimethylCyclopropane	4.502	$C_{10}H_{22}O$	158.28	27.65
5	1,4,7,10,13,16-Hexaoxacyclooctadecane	5.133	$C_{12}H_{24}O_6$	264.31	0.94
6	Urethane	5.396	$C_3H_7NO_2$	89.09	2.65
7	2-hydroxy2-Propen-1-amine	5.696	C_3H_7NO	73.09	7.51
8	2,4-Dimethylpentan-3-yl ethyl carbonate	6.453	$C_{10}H_{20}O_3$	188.26	1.07
9	Hexanoic acid	7.085	$C_6H_{12}O_2$	116.16	0.51
10	Cathinone	9.493	$C_9H_{11}NO$	149.19	0.10
11	Thymol	12.221	$C_{10}H_{14}O$	150.22	8.53
12	5-Dodecene	12.471	$C_{12}H_{24}$	168.32	4.68
13	Dodecanoic acid, methyl ester	12.740	$C_{13}H_{26}O_2$	214.34	2.34
14	1H-Indole-3-ethanamine	12.809	$C_{10}H_{12}N_2$	160.22	5.00
15	2(4H)-Benzofuranone	13.203	$C_8H_6O_2$	134.13	1.78
16	Methyl tetradecanoate	13.572	$C_{15}H_{30}O_2$	242.4	1.27
17	Dihydroactinidiolide	14.047	$C_{11}H_{16}O_2$	180.24	2.85

RT retention time
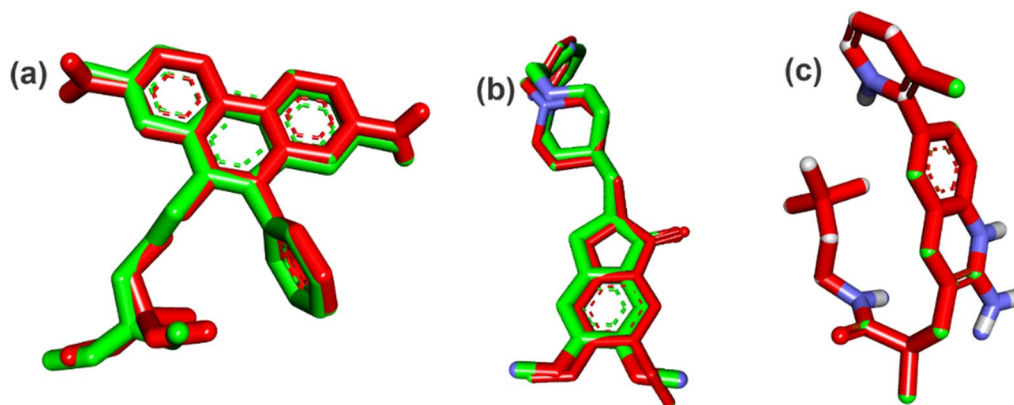
Fig. 3 Superimposed docked conformer of the native ligand on the extracted conformation of **a** propidium, **b** donepezil, **c** aminoquinoline compound 1. *Green: co-crystalized ligand conformer and red: selected docked conformer*

by only hydrophobic interactions. The phenol ring of thymol formed 2 Pi–Pi T-shaped contacts with Trp86 and Tyr337 of hAChE. The isopropyl unit made 2 Pi-sigma contacts with Trp86 and a Pi–Pi stacking with Trp86. The 5-methyl group made 2 Pi-sigma contacts with Phe338 and Tyr341 and a Pi-alkyl contact with Tyr337.

Analysis of the reference compound for hBChE shows that the docked propidium was deeply oriented in the active site of hBChE. The phenanthridinium ring was fitted into the groove of the acyl-binding pocket (Fig. 5). The ring one of the phenanthridine moiety made a Pi-donor hydrogen bond and a Pi–Pi T-shaped contact with

Trp231, and the Ser198 residue formed an H-bond with the amino group of the same ring. A Pi-sigma and Pi–Pi T-shaped contact was observed between the first and second rings with residues Leu286 and Phe329, respectively. A Pi–Pi T-shaped interaction stabilized the 6-phenyl moiety linked to the phenanthridinium ring with Tyr332 of the P-Site. Glu197 and Trp82, respectively, formed an attractive charged interaction and a Pi-cation contact with the nitrogen atom of the azane moiety (Fig. 5). The oxygen of the benzofuran-2-one of dihydroactinidiolide formed a hydrogen bond with Tyr128 of hAChE. Trp82 made 2 Pi-sigma contacts with the benzene ring of the

Table 3 Binding energies of the GC–MS identified phytochemicals from the *n*-hexane fraction of G. latifolium leaf extract and reference compounds that were docked in the active sites of *human* acetylcholinesterase, *human* butyrylcholinesterase and *human* β-secretase and Aβ fibrils

S no.	Compounds	Binding energy (Kcal/mol)			
		*h*AChE	*h*BACE1	*h*BChE	*h*Aβ fibrils
S2	DME601	− 6.7	− 7.7	− 5.3	− 6
S3	ED20	− 12.2	− 6.2	− 7.6	− 10.4
S4	Comp 1			− 7.6	
17	Dihydroactinidiolide	− 8	− 7.7	− 7.1	− 9.1
11	Thymol	− 7.5	− 6.8	− 6.2	− 8.3
16	Methyl tetradecanoate	− 7.2	− 6.2	− 5.4	− 8.5
14	1H-Indole-3-ethanamine	− 7.1	− 6.8	− 6.7	− 8.9
5	1,4,7,10,13,16-Hexaoxacyclooctadecane	− 6.8	− 2.8	− 6.6	− 8.4
10	Cathinone	− 6.8	− 6.5	− 6	− 8.2
15	2(4H)-Benzofuranone	− 6.8	− 6.8	− 6.2	− 8.3
8	2,4-Dimethylpentan-3-yl ethyl carbonate	− 6.7	− 5.8	− 5.4	− 7.9
13	Dodecanoic acid, methyl ester	− 6.4	− 6.2	− 5.5	− 7.7
12	5-Dodecene	− 6	− 6.2	− 5.3	− 7.1
9	Hexanoic acid	− 5.7	− 5.1	− 4.8	− 7.1
1	2,5-Dihydro-5-methoxy-2-furanone	− 5	− 4.6	− 4.8	− 7
4	1-Octanol, 3,7-dimethylCyclopropane	− 4.2	− 4.2	− 3.9	− 8.7
6	Urethane	− 4.1	− 3.7	− 3.8	− 6.7
3	1,3-Dimethyldiaziridine	− 3.9	− 3.4	− 3.7	− 6.7
2	Carbamic acid	− 3.4	− 3.2	− 3.1	− 6.5
7	2-hydroxy2-Propen-1-amine	− 3.4	− 3.0	− 3.4	− 5.4

S reference compound, *h*AChE *human* acetylcholinesterase, *h*BChE human butyrylcholinesterase, *h*BACE1 *human* β-secretase

Table 4 Amino acid interactions of *human* acetylcholinesterase, *human* butyrylcholinesterase, human β-secretase and *human* Aβ fibrils with the reference inhibitors and lead phytochemicals

	Protein	Hydrogen bonds		Hydrophobic Interaction	
		Numbers	Interacted residues	Numbers	Interacted residues
Donepezil	*h*AChE	1	Phe295	2	His447 Trp86 Trp286 Tyr341 Trp286 Phe338 Tyr337
Dihydroactinidiolide		1	Gly122	10	His447 Phe338 (3) Trp337 (3) Tyr341 (3)
Thymol		4		3	Trp86 (3) Tyr337 (3) Phe338 Tyr341
Propidium	*h*BACE1	2	Ser198 Trp231	7	Tyr332 Phe329(2) Leu 286 Trp231 Trp82 Glu197
Dihydroactinidiolide			Tyr128	3	Trp82 (2) His483 (2)
1H-Indole-3-ethanamine		2	Tyr128 Glu197	6	Trp82 (2) His483 (2)
Compound 1	*h*BACE1	5	Asp32(2) Gly34Asp228(2)	8	Tyr71(5) Val69(2)Phe108
Dihydroactinidiolide		6	Trp76	6	Tyr71(4) Val69 Phe108
1H-Indole-3-ethanamine		2	Phe108 Lys107	12	Leu30 Val69 Tyr71(3) Trp76 Trp115 Ile126 Tyr71(2) Trp76
Dihydroactinidiolide	*h*Aβ fibrils	1	Gln15	3	Ala21 Leu34 Val36
1H-Indole-3-ethanamine			AGln15 ALys15 AAla21	5	ALeu AGlu22 Aval36 Val36 Leu34

*h*AChE *human* acetylcholinesterase, *h*Aβ fibrils *h*Aβ fibrils, *h*BChE *human* butyrylcholinesterase, hBACE-1 *human* β-secretase and

benzofuran-2-one aglycon and a Pi-sigma contact with the 4 methyl group. His438 formed three pi-alkyl contacts with 4-methyl, 7-methyl and the benzofuran-2-one ring. The interaction between 1H-indole-3-ethanamine and hAChE was stabilized by two H-bonds. The nitrogen atom of the indole ring and that of the ethanamine moiety formed two H-bonds with Glu197 and Tyr128. The indole ring was oriented toward the A-site, where His438 and Trp82 formed 2 Pi-Cation and Pi-Pi stacking with the first and second rings of the indole ring, respectively.
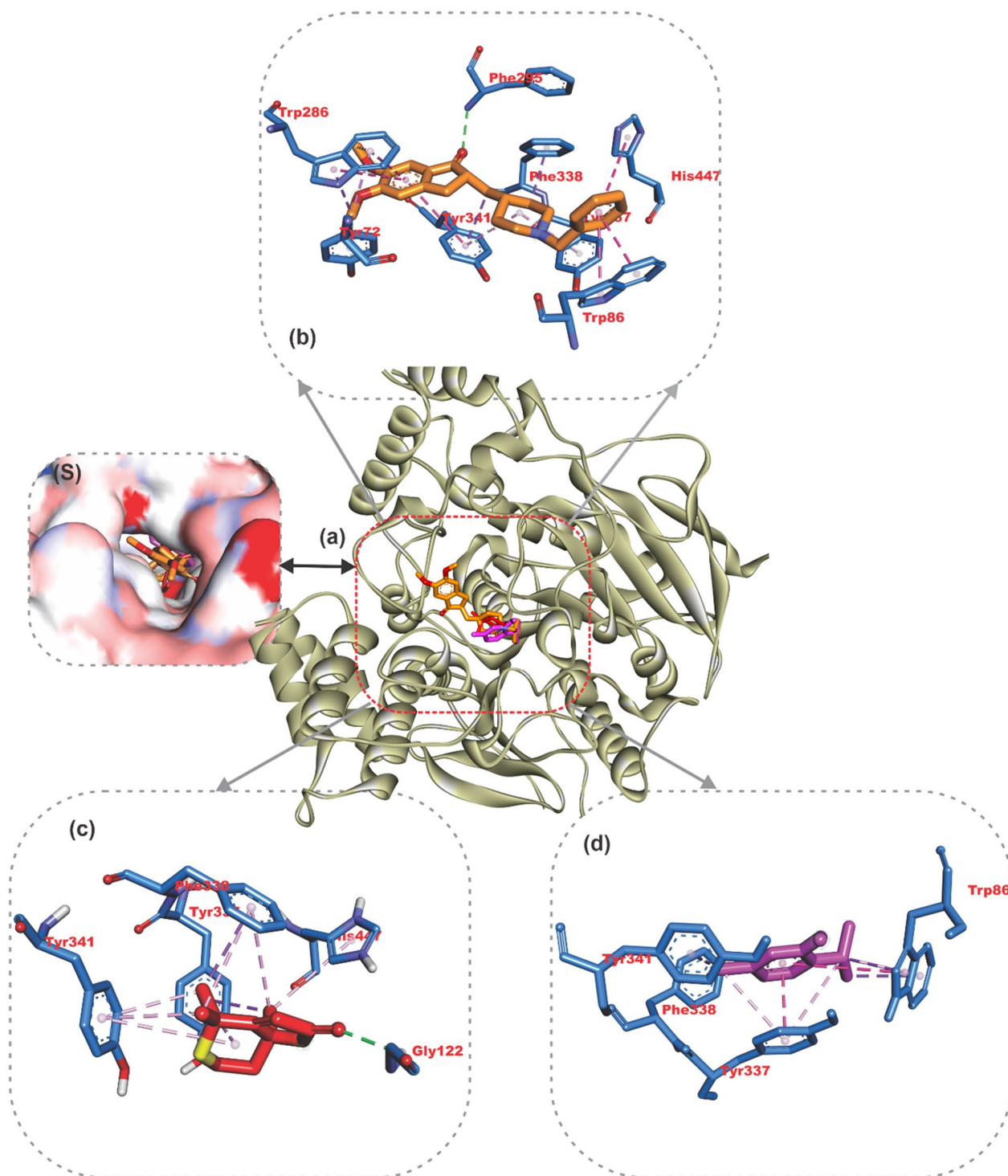
Fig. 4 Amino acid interactions of lead GC–MS identified phytochemicals from the *n*-hexane extract of *Gongronema latifolium* and reference inhibitor in the active site of *h*AChE **a** cartoon representation (S) surface-accessible representation. The ligands are presented in stick representation as shown in colors **b** gold: donepezil, **c** red: dihydroactinidiolide, **d** purple: thymol
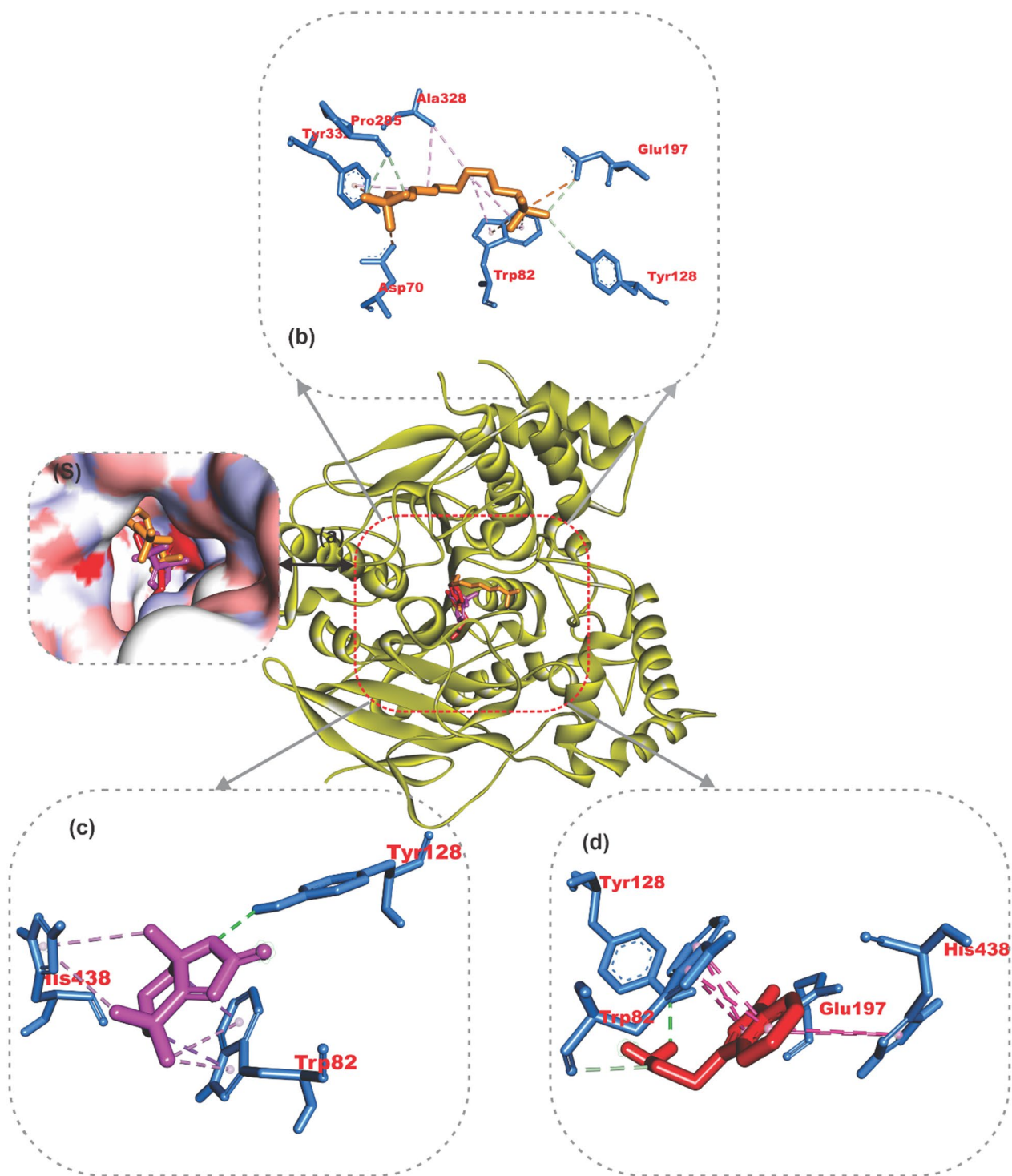
Fig. 5 Amino acid interactions of lead GC–MS identified phytochemicals from the *n*-hexane extract of *Gongronema latifolium* and reference inhibitor in the active site of *human* butyrylcholinesterase **a** cartoon depiction (S) surface-accessible representation The ligands are presented in stick representation as shown in colors **b** gold: propidium (reference inhibitor), **c** purple: dihydroactinidiolide, **d** red: 1H-Indole-3-ethanamine

In a comparable pattern of binding, the lead phytochemicals were positioned in the gorge of hBChE as propidium did. They interacted with the P-sites residue Tyr332 (Tyr341 in hAChE) and the A-sites residues Trp82, Trp231 and Phe329 (which are, respectively, Trp86, Trp236 and Phe338 in hAChE). Amino acid residues Asp70 and Trp82 have been involved in the catalytic machinery of hBChE. Therefore, compounds that interact in a similar way with these residues, just like propidium, will inhibit the catalytic action of the human butyrylcholinesterase (Fig. 5).

The aminoquinoline (3-(2-amino-6-(3-methylpyridin-2-yl)quinolin-3-yl)-*N*-(3,3-dimethylbutyl)-2-methylpropanamide) reference compound (1) exhibited the same pose with the exact pattern as the co-crystallized compounds. The compound was oriented in the S1' and S2' subpockets of the protein while leaving the S3 and S3 subpocket (sp) accessible to hBACE1 (Fig. 6). Dihydroactinidiolide was accommodated in the same region as the reference inhibitor. The bonding was stabilized by the only carbon-hydrogen bond between the benzene ring and Trp76 and several hydrophobic interactions. 7α-Methyl group of dihydroactinidiolide formed two alkyl contacts with Val69 and Tyr71. Tyr71 made alkyl, Pi-Sigma and Pi-alkyl contacts to 4-methyl, 4'-methyl groups and benzofuran-2-one rings, respectively. The benzene ring of the benzofuran-2-one moiety interacted via pi-alkyl contact with Phe108 of hBACE1. Two conventional hydrogen bonds were formed by the amino group of the 2-aminoethyl group that is linked to the indole ring of 1H-indole-3-ethanamine. The first and second rings of the indole moiety formed several Pi–Pi T stackings and Pi–Pi stackings with Phe108, Trp76 and Try71 residues, which are part of the flap region of BACE-1 (Fig. 6).

An exhaustive blind docking was performed around the pentameric Aβ fibrils (2BEG) in order to ascertain potential high-affinity binding regions of the phytochemicals within the fibrils. The amino acid interactions of the high binding region are represented in Table 4. Dihydroactinidiolide and 1H-indole-3-ethanamine interacted with the pentameric Aβ fibrils with the greatest binding affinity. Dihydroactinidiolide was stabilized in the fibril by a hydrogen bond to Gln15 and alkyl interactions between the benzene ring of the benzofuran-2-one moiety and Ala21, Val36 and Leu34. The two amino nitrogens of the 2-aminoethyl group of 1H-indole-3-ethanamine formed 2 hydrogen bonds to Ala21A and Lys16A of the first fibril, while the nitrogen of the indole ring formed another hydrogen bond to Gly15A of the first fibril. The interaction in the indole ring was stabilized by several hydrophobic interactions, including Pi-sigma contact with Leu34,

amide-Pi stacking with Ala21A and Pi-alkyl contacts with Ala21A, Leu34A and Val36A (Fig. 7).

Ensemble-based docking interactions of phytochemicals with representative conformations from MD simulation trajectories of target proteins

In order to perform ensembled-based molecular docking analysis in which the GC–MS identified phytochemicals were docked to various conformers of the unbound proteins that were obtained from the full 100 ns atomistic MD simulation of the unbound hAChE, hBChE, and hBACE1, while a 500-ns MD simulation trajectory for hAβ fibrils [57] was used for the cluster investigation. The TTClust clustering analysis of the MDS trajectories of apo proteins produced 3, 4, 2 and 4 different clusters for *h*AChE, *h*BChE, *h*BACE1 and *h*Aβ fibrils, respectively, from the different frames. From the generated clusters for each protein, a representative structure was generated and utilized in the ensemble docking investigation used for the cluster investigation.

The TTClust clustering analysis of the MDS trajectories of apo proteins produced 3, 4, 2 and 4 different clusters for hAChE, hBChE, hBACE1 and hAβ fibrils, respectively, from the different frames. From the generated clusters for each protein, a representative structure was generated and utilized in the ensemble docking investigation. The TTClust clustering analysis of the MDS trajectories of apo proteins produced 3, 4, 2 and 4 different clusters for hAChE, hBChE, hBACE1 and hAβ fibrils, respectively, from the different frames. From the generated clusters for each protein, a representative structure was generated and utilized in the ensemble docking investigation. The mean binding energies of the phytochemicals for hAChE, hBChE, hBACE1 and hAβ fibrils range from -6.525 to -3.6, -6.833 to -3.5, -6.2 to -3.4 and -6.325 to -3.15 kcal/mol, respectively. From the ensemble-based docking analysis, the top two phytochemicals with the highest binding energy were chosen as the lead phytochemicals for further interactive analysis. Dihydroactinidiolide $(-6.525 \pm 0.895$ kcal/mol) and 1H-Indole-3-ethanamine $(-6.475 \pm 0.985$ kcal/mol) were the lead phytochemicals for hAChE. This was slightly different from the initial docking analysis, where thymol was the second-leading phytochemical for hAChE. Dihydroactinidiolide and 1H-Indole-3-ethanamine were the lead phytochemicals for the three other protein targets, with -6.833 ± 0.461 and -6.466 ± 0.577 kcal/mol for hBChE, -6.2 ± 0.845 and -5.95 ± 0.353 kcal/mol for hBACE1 and -6.325 ± 0.221 and -5.925 ± 0.05 kcal/mol for hAβ fibril. This is in accordance with the initial docking analysis. The complexes containing the
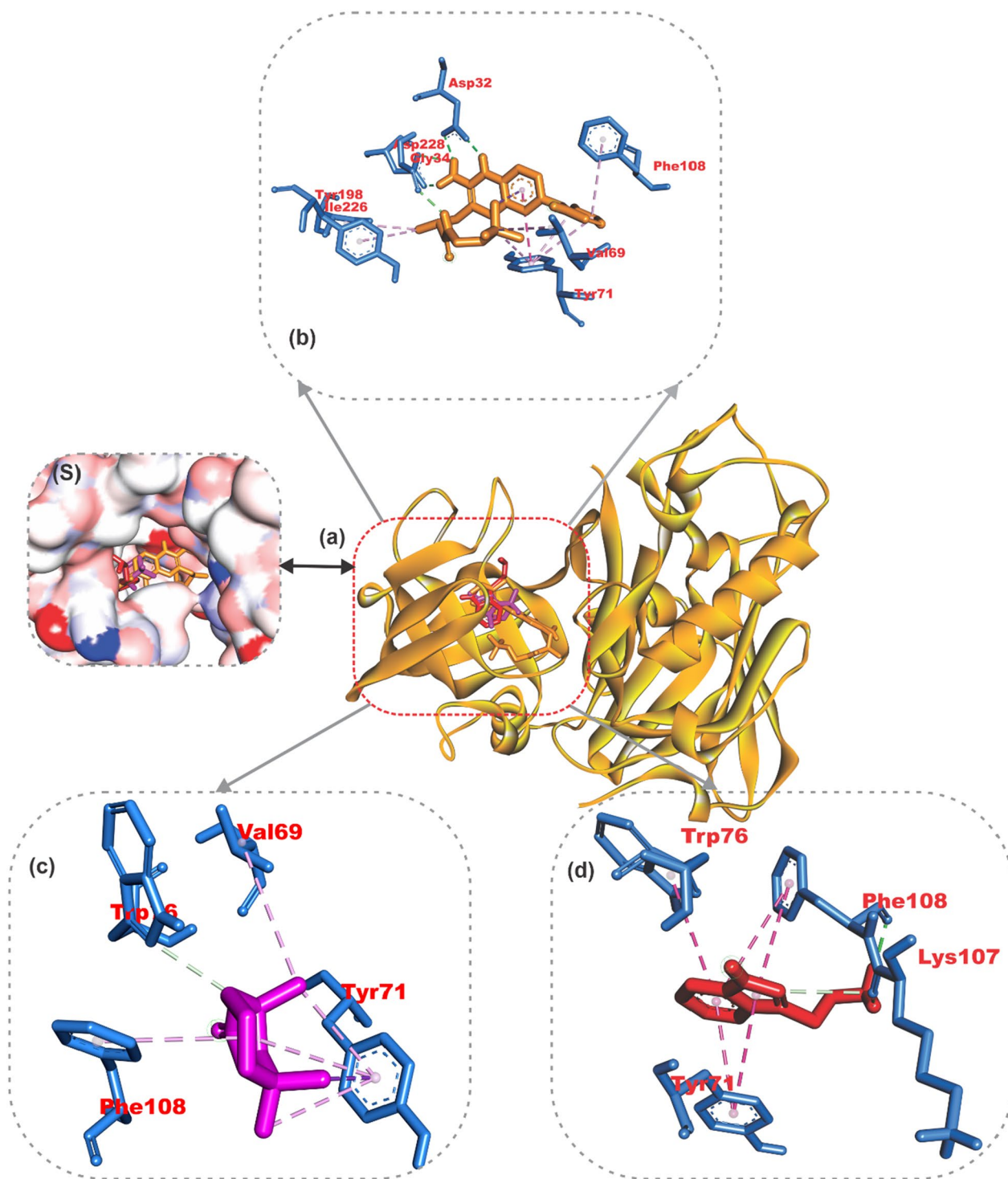
Fig. 6 Amino acid interactions of lead GC–MS identified phytochemicals from the *n*-hexane extract of *Gongronema latifolium* and reference inhibitor in the active site of *human* BACE-1 **a** cartoon illustration (S) surface-accessible representation. The ligands are presented in stick representation as shown in colors **b** gold: compound 1 (reference inhibitor), **c** purple: dihydroactinidiolide, **d** red: 1H-Indole-3-ethanamine
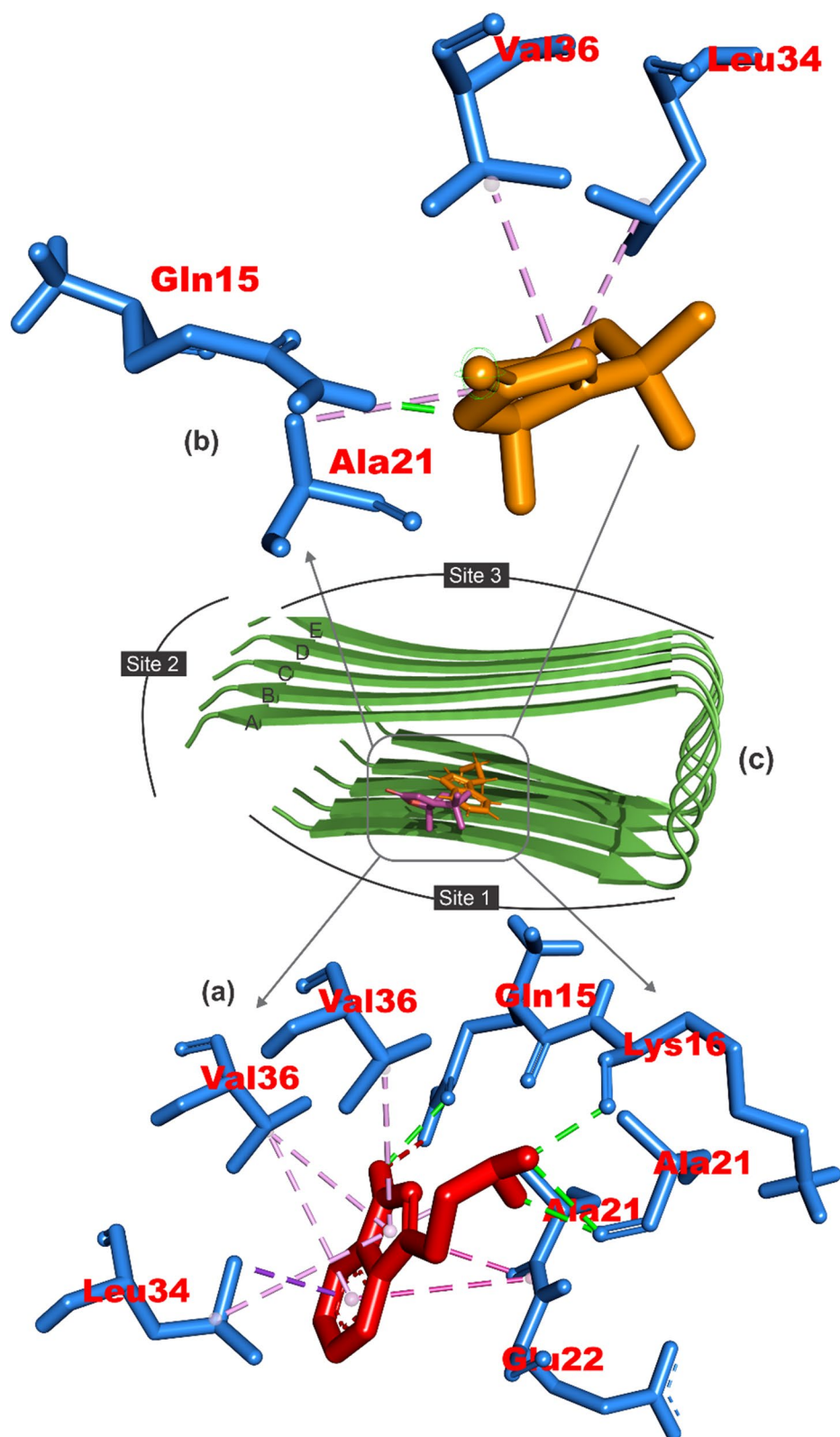
Fig. 7 Amino acid interactions of lead GC–MS identified phytochemicals from the *n*-hexane extract of *Gongronema latifolium*. The ligands are presented in stick representation as shown in colors **a** gold: 3D interactive view of dihydroactinidiolide; **b** red: 3D interactive view of 1H-Indole-3-ethanamine. In the binding site 1 of Aβ fibrils. **c** Cartoon depiction of the best docked match of lead phytochemicals in the binding site 1 of Aβ fibrils

Table 5 The interactions of the 2 lead phytochemicals and reference inhibitors with the best representative structures from the cluster analysis

Protein	Compound	Binding energies (kcal/mol)	H-bonding		Hydrophobic interactions	
			Number	Residues	Number	Residues
*h*AChE	Donepezil	−8.1	4	Cys145 His41 Leu167 Glu166	2	Met165 Pro168
	Dihydroactinidiolide	−7.5	5	Gly143 Ala191 Thr26	1	Pro168(2), Leu167, Cys145
	1H-Indole-3-ethanamine	−6.9	3	Arg188 Thr190 Pro168	1	Leu167 Met165 Cys145
*h*BChE	Propidium	−5.9	3	Cys270 Asn142 Gly271	2	Trp106 Asn109
	Dihydroactinidiolide	−7.1	6	Gln269 Cys270 Ans267 Trp106 His272 Asn109	4	Trp106 (2) Lys94 Ala107
	1H-Indole-3-ethanamine	−6.8	4	Gln269 Asn109 Cys270 Trp106	5	Lys92 Ala107 Trp93 Lys94 Lys105
*h*BACE1	Compound 1	−6.8	4	Asp32 (2) Tyr71 Pro70	4	Tyr123 Trp197 Tyr198 Ile226
	Dihydroactinidiolide	−6.8	1	Arg128	3	Trp197(3)
	1H-Indole-3-ethanamine	−6.2	2	Glu125 Tyr123	1	Trp197
*h*Aβ	Dihydroactinidiolide	−6.6	3	Gln15A Val18A Leu17A	4	Ala21C Phe19A Val24D Val18D
	1H-Indole-3-ethanamine	−6.6	3	Val18A Phe19D Ala21D	5	Val18D Ala21C Glu22C Leu17A

representative conformer with the greatest binding affinity for the lead phytochemicals were selected for further interactive analysis. The interacting amino acids of the proteins with lead phytochemicals are presented in Table 5. The amino acid interactions with the lead phytochemicals in the selected cluster were similar to those observed from static docking (Fig. 8).
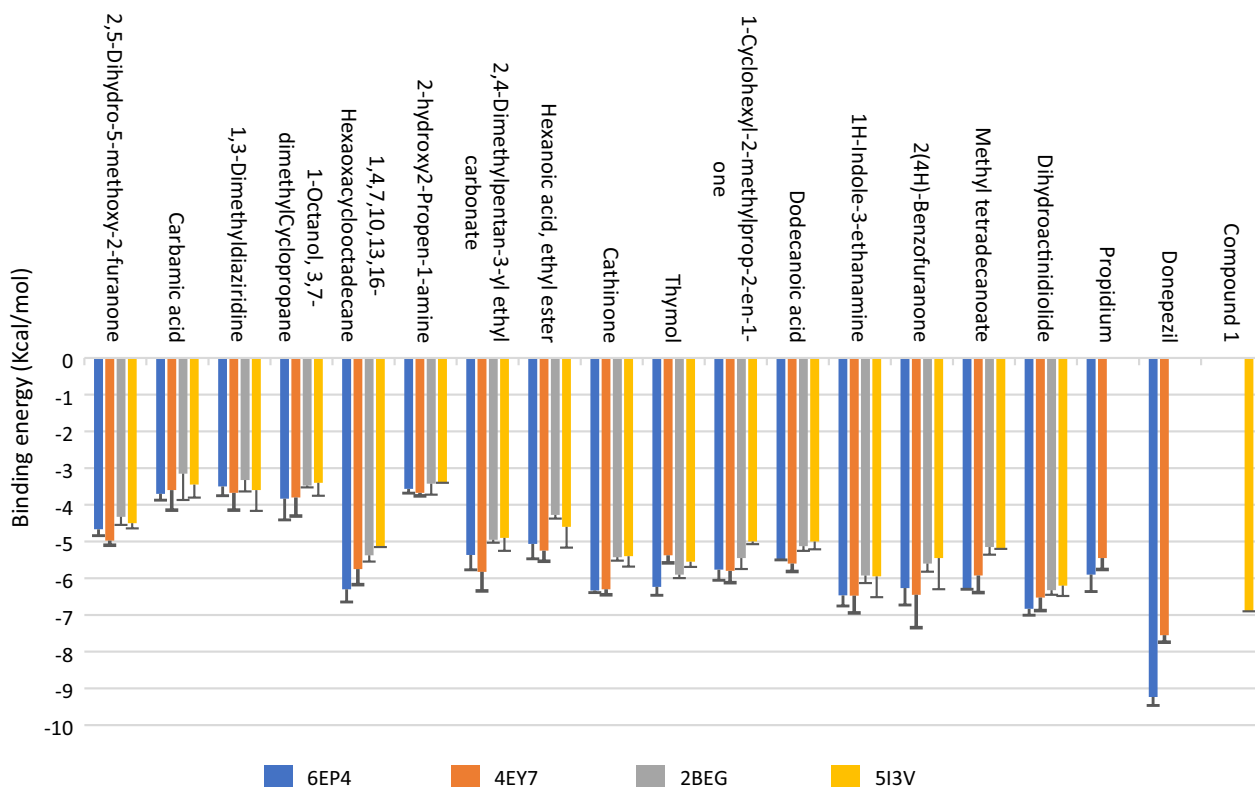

Fig. 8 The binding energies mean and STD of selected phytochemicals and reference inhibitors and docked against conformation acquired from the cluster analysis of the trajectories obtained from the MD simulation of *h*AChE, *h*BChE, *h*BACE1 and *h*Aβ fibrils. Number of clusters: *h*AChE = 3, *h*BChE = 4, *h*BACE1 = 2 and *h*Aβ = 4. The error bars denote the STD (standard deviation)
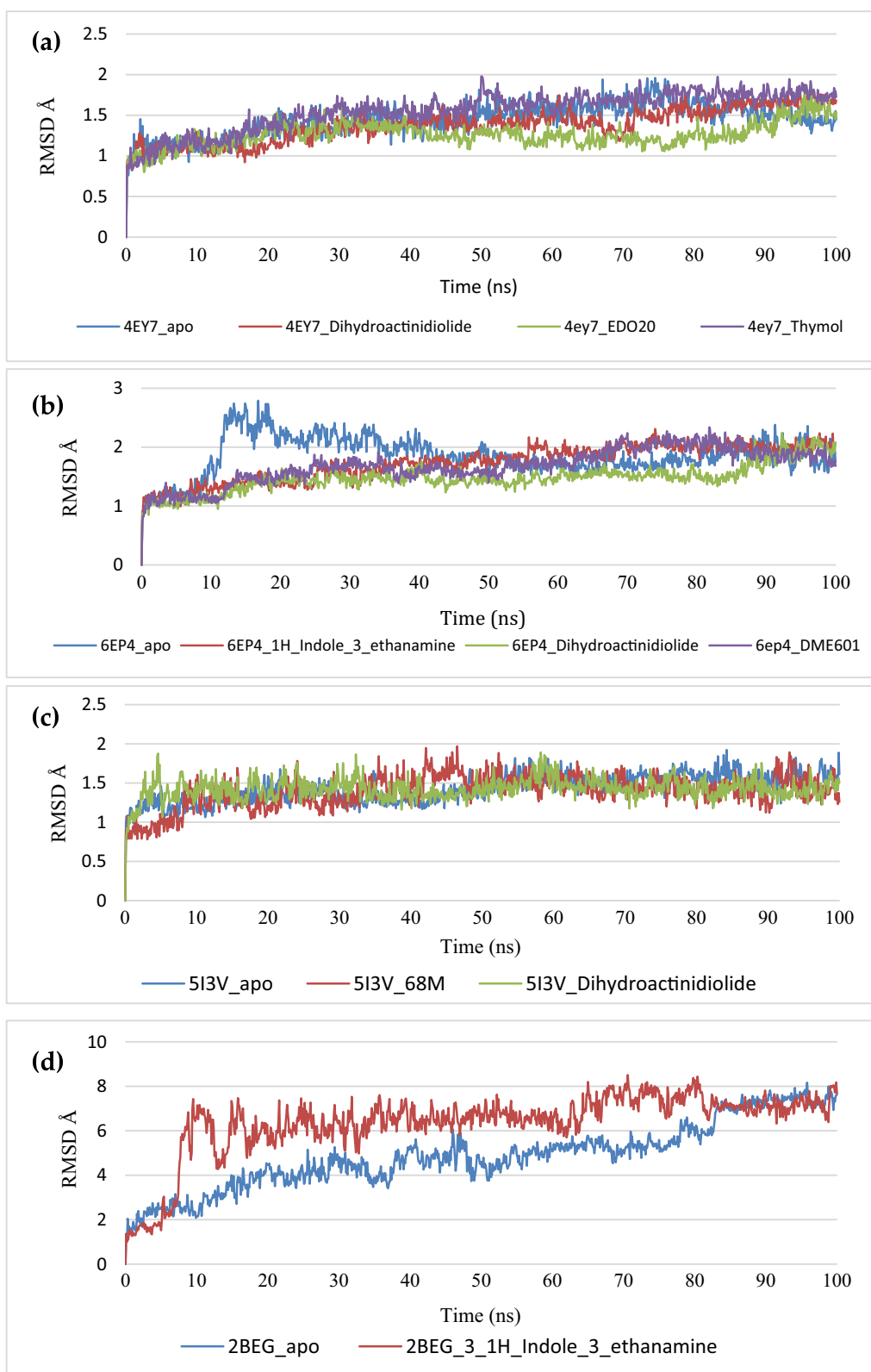
Fig. 9 The backbone RMSD plots of molecular dynamics simulation of selected ligands complexed to **a** *h*AChE, **b** *h*BChE, **c** *h*BACE1, **d** *h*Aβ fibrils

Molecular dynamics simulation of lead complexes

Figure 9 shows the plots for the RMSD parameters of the three enzyme systems. The systems experienced equilibrated about 10 ns and continued with very minimal fluctuations until the end of the simulation. The *h*AChE systems demonstrated the same pattern of RMSD with average RMSD values of 14428, 1.2623, 1.3821 and 1.5512 Å for the apo enzyme, donepezil, dihydroactinidiolide and thymol complexes, respectively (Fig. 9a). The *h*BChE systems had average RMSD values of 1.8590, 1.6811, 1.4731 and 1.7323 Å for the unbound enzyme, propidium, dihydroactinidiolide and 1H_Indole_3_ethanamine complexes, respectively (Fig. 9b). The systems for the BACE-1 enzyme had mean RMSD values of 1.4234, 1.3948, 1.3539 and 1.4255 Å for the apo protein, compound 1, Indole_3_ethanamine and dihydroactinidiolide complexes, respectively, while the mean RMSD values for the *h*Aβ are 4.8708 and 6.3524 Å for the apo and 1H_Indole_3_ethanamine (Fig. 9c). It was noted that the binding of the lead compounds to *h*AChE, *h*BChE and BACE-1 caused a decline in the mean RMSD amount when related to the unbound protein; the binding of 1H-Indole-3-ethanamine to the *h*Aβ fibril increased the mean RMSD value when compared to the unbound. The hAChE systems had a mean RMSF values of 0.8400, 0.8064, 0.8349 and 0.8284 Å for the apo protein donepezil, dihydroactinidiolide and thymol (Fig. 10a). The hBChE system presented mean RMSF values 0.9531, 0.8753, 0.8791 and 0.8745 Å for the apo enzyme, propidium, dihydroactinidiolide and 1H_Indole_3_ethanamine complexes (Fig. 10b). The apo enzyme for the BACE-1 systems presented average RMSF values of 0.8464 Å, while the enzyme complexed with compound 1, 1H-Indole-3-ethanamine and dihydroactinidiolide had 0.7587, 0.8509 and 0.7780 Å as their mean RMSF values (Fig. 10c), while the apo and 1H-Indole-3-ethanamine *h*Aβ systems had 2.8524 and 2.3222 Å as their mean RMSF value (Fig. 10d).

The RoG designs of the systems are shown in Fig. 11. The plots for the systems show a stabilized progression after equilibration throughout the time of the simulation period, while the *h*BChE and BACE-1 systems presented minimal fluctuations. The *h*AChE presented is 23.1398, 23.1825, 23.1282 and 23.1209 Å for the unbound enzymes, donepezil, dihydroactinidiolide and thymol (Fig. 11a). The *h*BChE system presented mean RoG values 23.2362, 23.2114, 23.2216 and 23.2651 Å for the apo enzyme, propidium, dihydroactinidiolide and 1H_Indole_3_ethanamine complexes (Fig. 11b). The apo enzyme for the BACE-1 systems presented average RoG values of 0. 21.3970 Å, while the enzyme complexed with compound 1, 1H-Indole-3-ethanamine and dihydroactinidiolide had 21.3855, 21.4182 and 21.4056 Å as their mean RoG values (Fig. 11b), while the apo and 1H-Indole-3-ethanamine *h*Aβ systems had 14.9796 and 14.9209 Å as their mean RoG values (Fig. 11d). The unbound proteins systems presented close of average RoG values to the bound system, indicating compactness of the protein structures was not negotiated by the binding of the lead phytochemicals.

Furthermore, the degree of solvent accessibility is measured from the SASA plots. Both SASA and RoG are used to the reliability of the folded protein. The computed mean SASS values for the *h*AChE systems are 22,909.43, 23,156.54, 23,124.61 and 23,263.32 Å^2 for the unbound enzyme, donepezil, dihydroactinidiolide and thymol (Fig. 12a). The hBChE system presented mean SASA values 23,313.53, 23,542.71, 23,355.29 and 23,313.53 Å^2 for the apo enzyme, propidium, dihydroactinidiolide and 1H_Indole_3_ethanamine complexes (Fig. 12b). The apo enzyme for the BACE-1 systems presented average SASA values of 17,671.03, while the enzyme complexed with compound 1, 1H-Indole-3-ethanamine and dihydroactinidiolide had 17,660.65, 17,699.90 and 17,849.58 Å^2 as their mean SASA value (Fig. 12c), while the apo and 1H-Indole-3-ethanamine *h*Aβ systems had 8463.66 and 8393.52 Å^2 as their mean values. For all the four enzymes, the bound systems presented close SASA amounts when compared to the unbound protein.

The computed average number of H-bonds for the *h*AChE systems was 114.3826, 119.8561, 118.8002, 113.3656 for the freed enzyme, donepezil, dihydroactinidiolide and thymol. The mean number of H-bonds for the hBChE system is 123.9101, 122.3636, 123.9940 and 127.4345 for the apo enzyme, propidium, dihydroactinidiolide and 1H_Indole_3_ethanamine complexes. The average number of H-bonds for the BACE-1 system is 91.17, 90.32, 91.50 and 88.13 for the apo enzyme, compound 1, 1H-Indole-3-ethanamine and dihydroactinidiolide bound complexes, while the apo and 1H-Indole-3-ethanamine *h*Aβ systems had 25.64 and 26.43 (Fig. 13).

Molecular mechanics generalized born surface area (MMGBSA) analysis

The free energy of binding for the lead phytochemical to the corresponding protein targets was added using the MMGBSA methods. The results for hAChE, hBChE and BACE-1 and hAβ fibrils systems show that dihydroactinidiolide had the greatest binding free energy compared to the other lead compound, although not as high as the reference compounds. The investigation of various component of the total binding free energy is presented in Table 6. The breakdown of the total binding free based on contributory amino acid and the energy changes of the system throughout the simulation time of 100 ns is given
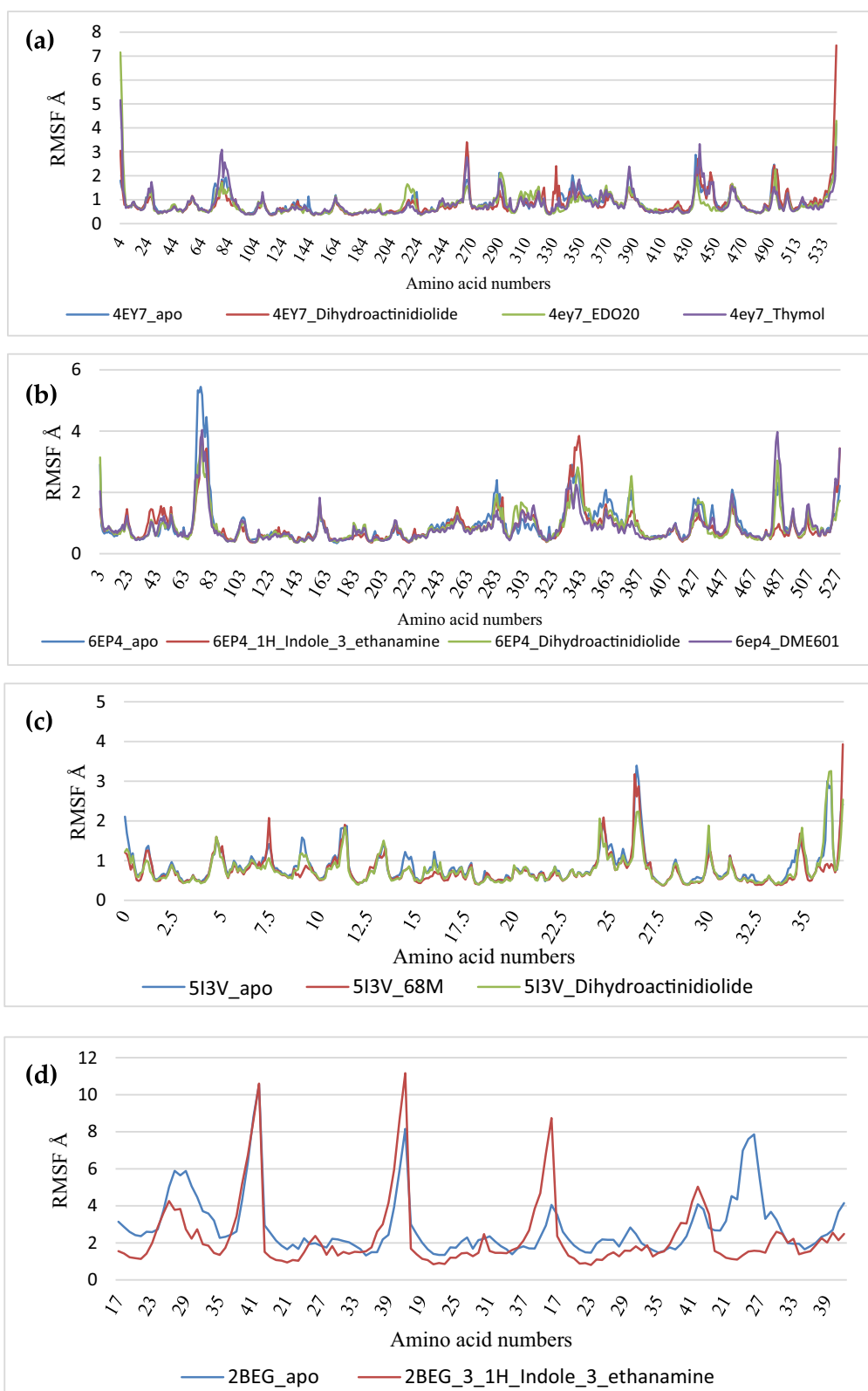
Fig. 10 Per residue RMSF plots of molecular dynamics simulation of selected ligands complexed to **a** *h*AChE, **b** *h*BChE, **c** *h*BACE1, **d** *h*Aβ fibrils
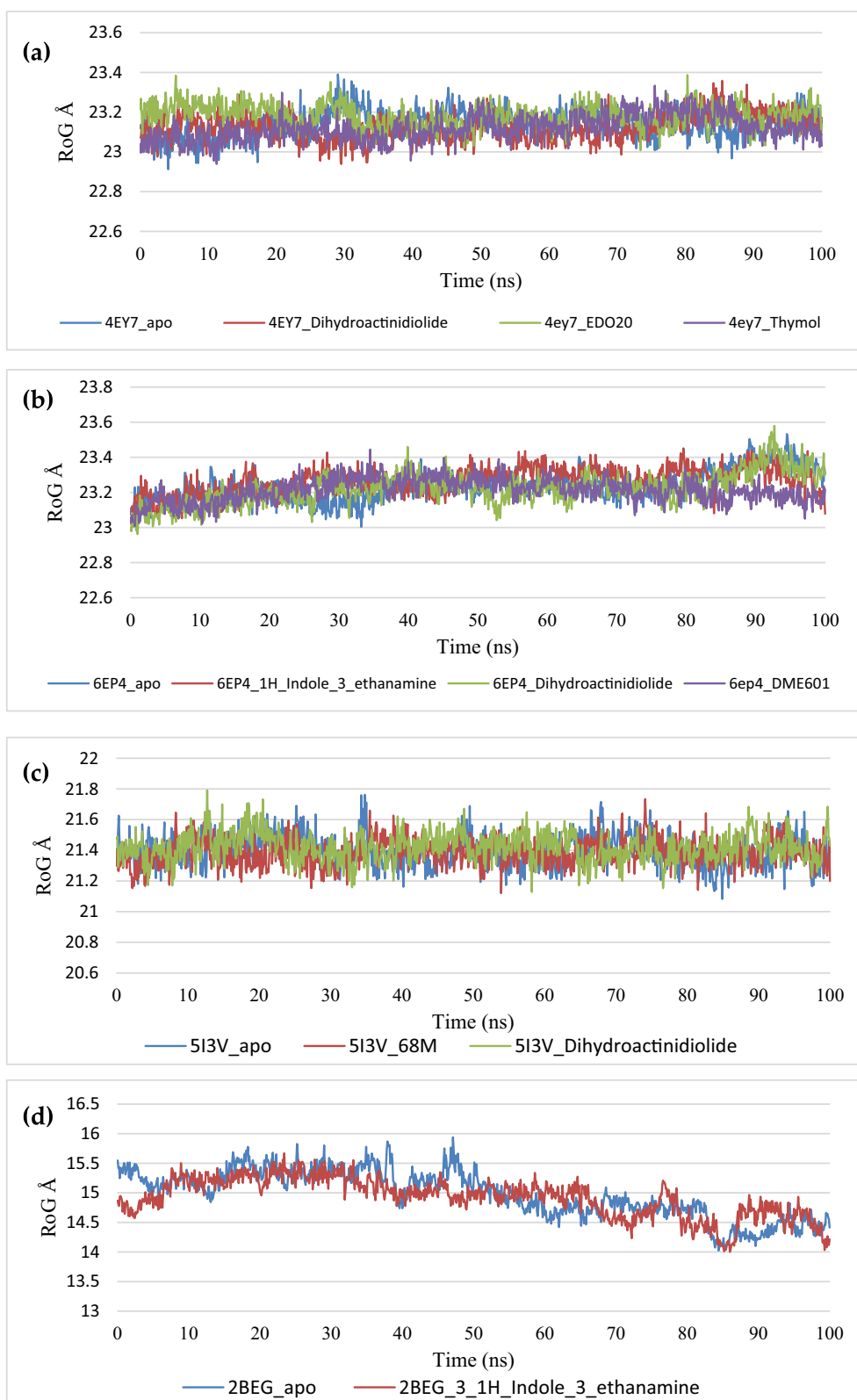
Fig. 11 RoG plots of molecular dynamics simulation of selected ligands complexed to **a** *h*AChE, **b** *h*BChE, **c** *h*BACE1, **d** *h*Aβ fibrils
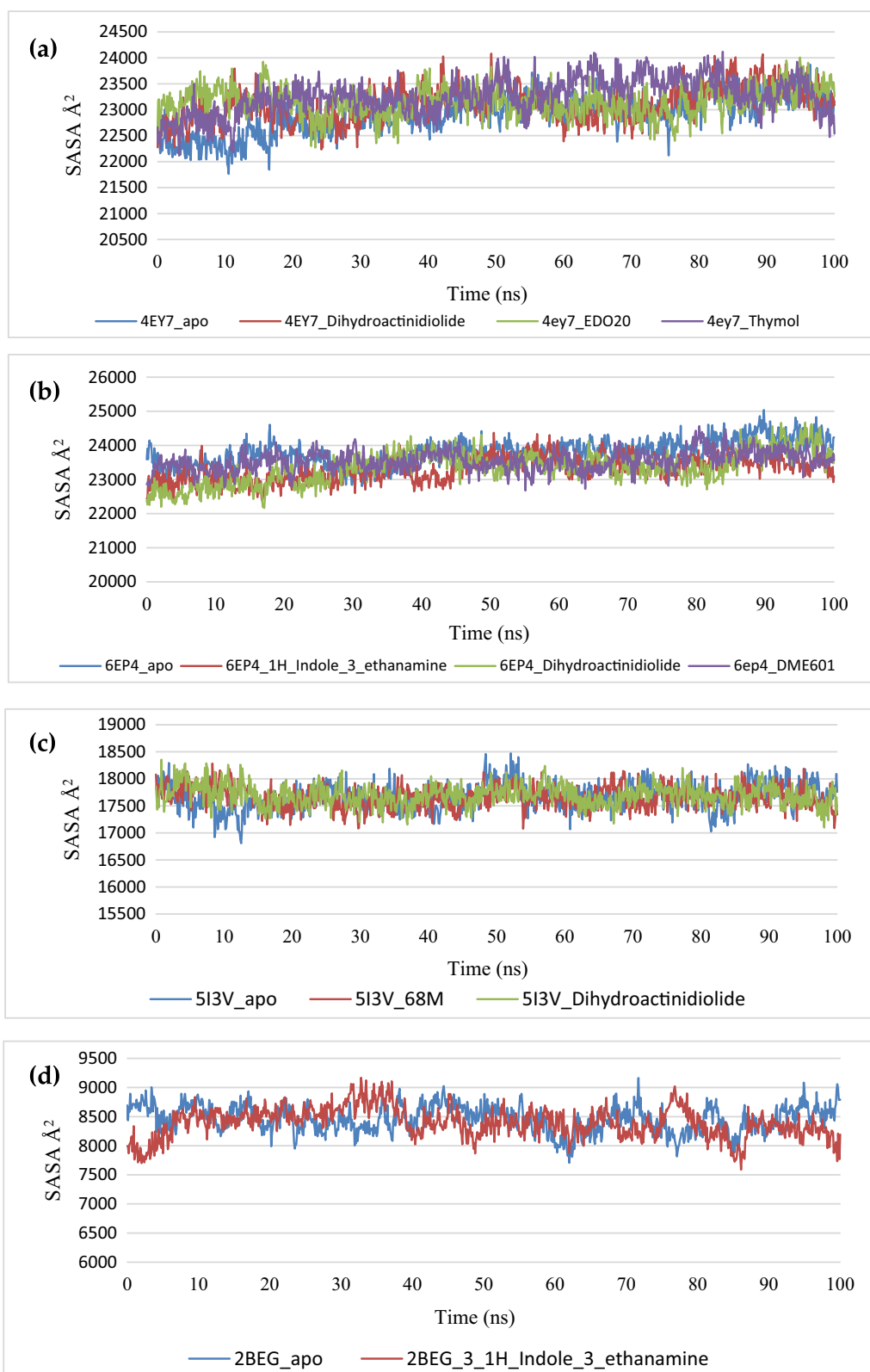
Fig. 12 The surface-accessible surface area (SASA) plots of molecular dynamics simulation of selected ligands complexed to **a** *h*AChE, **b** *h*BChE, **c** *h*BACE1, **d** *h*Aβ fibrils
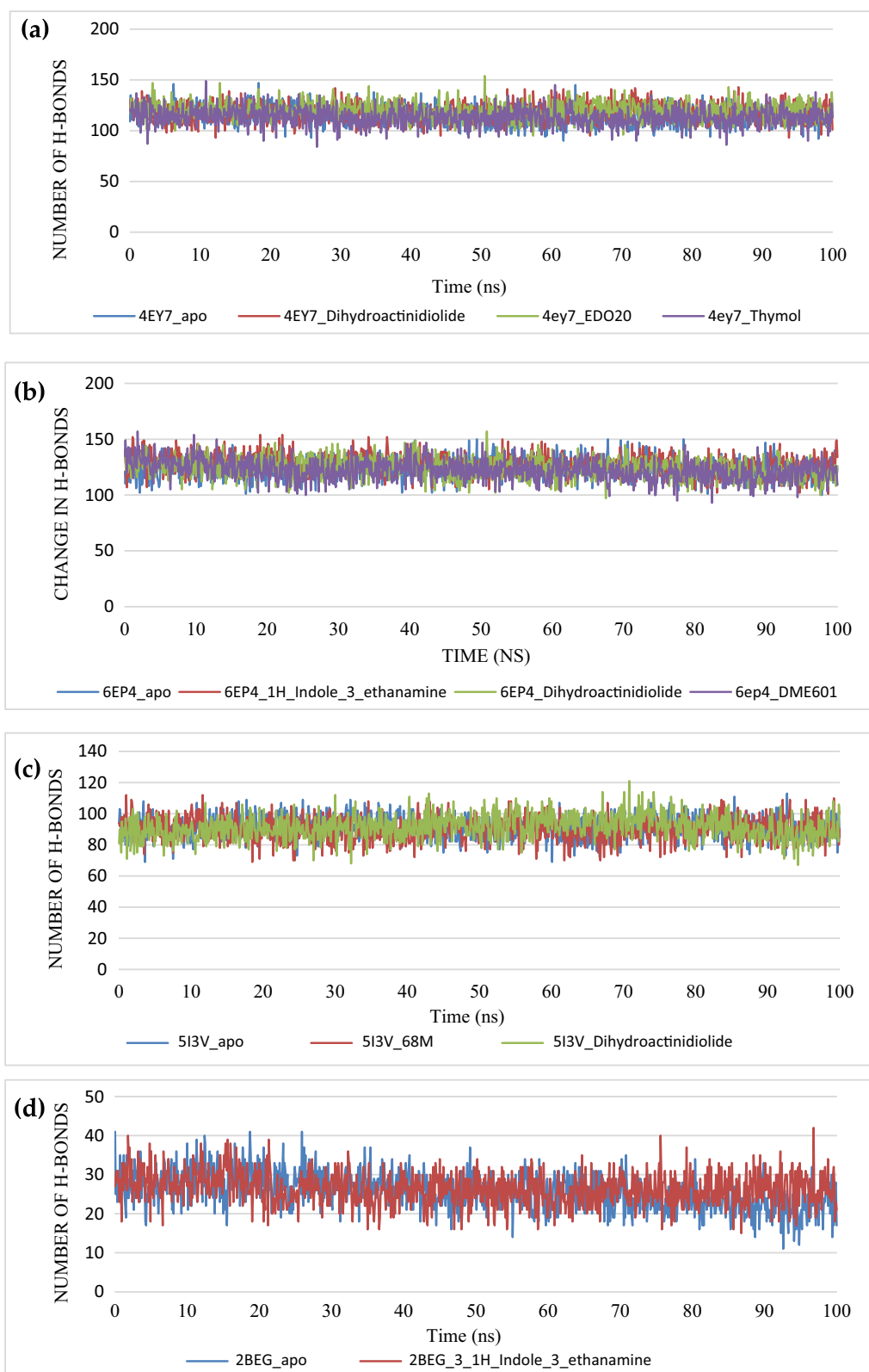
Fig. 13 The plots for showing the changes in the number of H-bonds during the MDS trajectory of selected ligands complexed to **a** *h*AChE, **b** *h*BChE, **c** *h*BACE1, **d** *h*Aβ fibrils

Table 6 Mean and SD of different energy constituents of the binding free energy of lead phytochemicals to respective proteins

System	$\Delta_{VDWAALS}$	Δ_{EEL}	Δ_{EGB}	Δ_{ESURF}	Δ_{GGAS}	Δ_{GSOLV}	Δ_{TOTAL}
4EY7_dihydroactinidiolide	−25.4±2.16	−11.64±3.83	22.12±3.50	−3.46±0.18	−37.04±5.08	18.66±3.44	−18.38±2.60
4EY7_ Donepezil	−44.37±2.80	−6.31±4.07	35.42±4.31	−6.07±0.32	−50.68±5.51	29.35±4.15	−21.33±3.19
4EY7_Thymol	−21.96±2.74	−7.35±4.31	16.82±2.51	−3.12±0.27	−29.31±3.87	13.7±2.51	−15.61±2.47
6ep4_1H-Indole-3-ethanamine	−21.57±2.08	−5.06±4.36	19.72±3.98	−3.04±0.26	−26.63±4.40	16.68±3.95	−9.95±2.24
6ep4_Dihydroactinidiolide	−19.84±2.80	−4.12±6.91	11.84±6.25	−2.82±0.37	−23.96±7.91	9.01±6.13	−14.95±3.47
6ep4_ Propidium	−26.51±5.26	−197.43±32.76	210.53±35.75	−4.23±0.88	−223.94±36.58	206.3±35.08	−17.64±3.93
5i3v_Comp 1	−41.34±2.87	−18.02±3.90	45.98±4.47	−5.58±0.36	−59.37±5.26	40.4±4.21	−18.96±2.86
5i3v_Dihydroactinidiolide	−18.3±1.97	−9.91±5.70	18.09±4.98	−2.81±0.28	−28.21±6.43	15.27±4.90	−12.94±2.61
2beg_1H-Indole-3-ethanamine	−20.64±2.23	−181.49±18.83	191.43±16.86	−3.39±0.15	−202.14±18.55	188.05±16.84	−14.09±3.19

in Figs. 14, 15, 16 and 17. It was noted that the interacting residues during the static docking were majorly involved in the contribution to the total binding free energy. Amino acid residues that contributed atleast −0.5 kcal/mol to the e total binding free energy for each system are listed below. 4EY7_dihydroactinidiolide (Trp82, Tyr124, Phe295, Phe297, Phe388, Tyr341); 4EY7_Thymol (Trp82, Val294, Arg296, Phe297, Tyr341) (Fig. 14); 6EP4_Dihydroactinidiolide (Val331, Tyr332, Trp340, Met434, Met437); 6EP4_1H-Indole-3-Ethanamine (G117, Leu286, Phef329, Tyr332) (Fig. 15); 5I3V_Dihydroactinidiolide (Leu30, Gln73, ILE110) (Fig. 16) and 2BEG_1H-Indole-3-Ethanamine (Ala21, Asp23, Ile32) (Fig. 17).

In silico drug-likeness and pharmacokinetic properties of top docked steroidal saponins
The three lead phytochemicals that were obtained from the docking and ensemble-based docking investigations were further evaluated in silico for predictive drug-likeness and ADMET (Absorption, Distribution, Metabolism, Excretion, and Toxicity) analyses over a wide range of filters and molecular descriptors. The results obtained from these analyses are represented in Table 7. Dihydroactinidiolide and 1H-Indole-3-ethanamine satisfied the requirements for the four drug-likeness filtering analyses (Lipinski, Veber, Ghose, and Egan), indicating that they are highly druggable, while thymol fulfilled the requirements for three of the filters of drug-likeness (Lipinski, Veber, Egan). The optimal range of the physiochemical parameters as provided by ADMETlab 2.0 is represented in Fig. 18 [58]. The three leading phytocompounds showed high gastrointestinal absorption, thereby suggesting high bioavailability. They showed the ability to traverse the brain-blood barrier, which is an important property of neurodegenerative drugs (Table 6). Dihydroactinidiolide, 1H-Indole-3-ethanamine and thymol were projected to be negative substrates of the P-glycoprotein with high plasma protein binding inclinations.

The effects of the lead phytochemicals on stage I drug metabolism in the liver were also analyzed using a wide range of molecular cytochrome P450 descriptors. The lead phytochemicals are projected not to show inhibitory potential for the cytochrome P450 descriptors. The predictive analysis further recommended that the lead phytochemicals were not mutagenic or carcinogenic and would not provoke skin sensitization. The predicted LD_{50}, clearance rate and half-life of the lead phytochemicals were in a satisfactory range (Table 7).

Discussion
The ethnobotanical use of *Gongronema latifolium* is for treating various forms of neurological disorders and evidence from the reported ethnopharmacological activities of different extracts of the leaf [30, 59]. Herein, we performed extraction of the methanol extract of the leaves, solvent–solvent partitioning of the methanol extract, monoamine and cholinesterase enzyme inhibitory assays, GC–MS profiling and numerous computational methods to decipher the possible neurotherapeutic constituents in the *n*-hexane partition fraction of *Gongronema latifolium* leaf. The concentration-dependent AChE and BChE inhibitory activities of the *n*-hexane solvent partition fraction (HF) of the methanol extract were in agreement with previous studies on the same leaf [30, 59]. Furthermore, it was observed that the HF of the methanol extract presented a higher percentage inhibition of the BChE compared to the AChE; this is desirable because, in the late stage of AD in humans, the predominating cholinesterase is BChE [60]. Additionally, the inhibition of BChE activity has been reported to decelerate the formation of neurotoxic plaques, which are implicated in the development of AD [61].

The GC–MS analysis of the HF of Gl extract showed that cambamic acid, 1,3-dimethyldiaziridine and 1-octanol, 3,7-dimethylcyclopropane were the most abundant compounds. Although several studies have
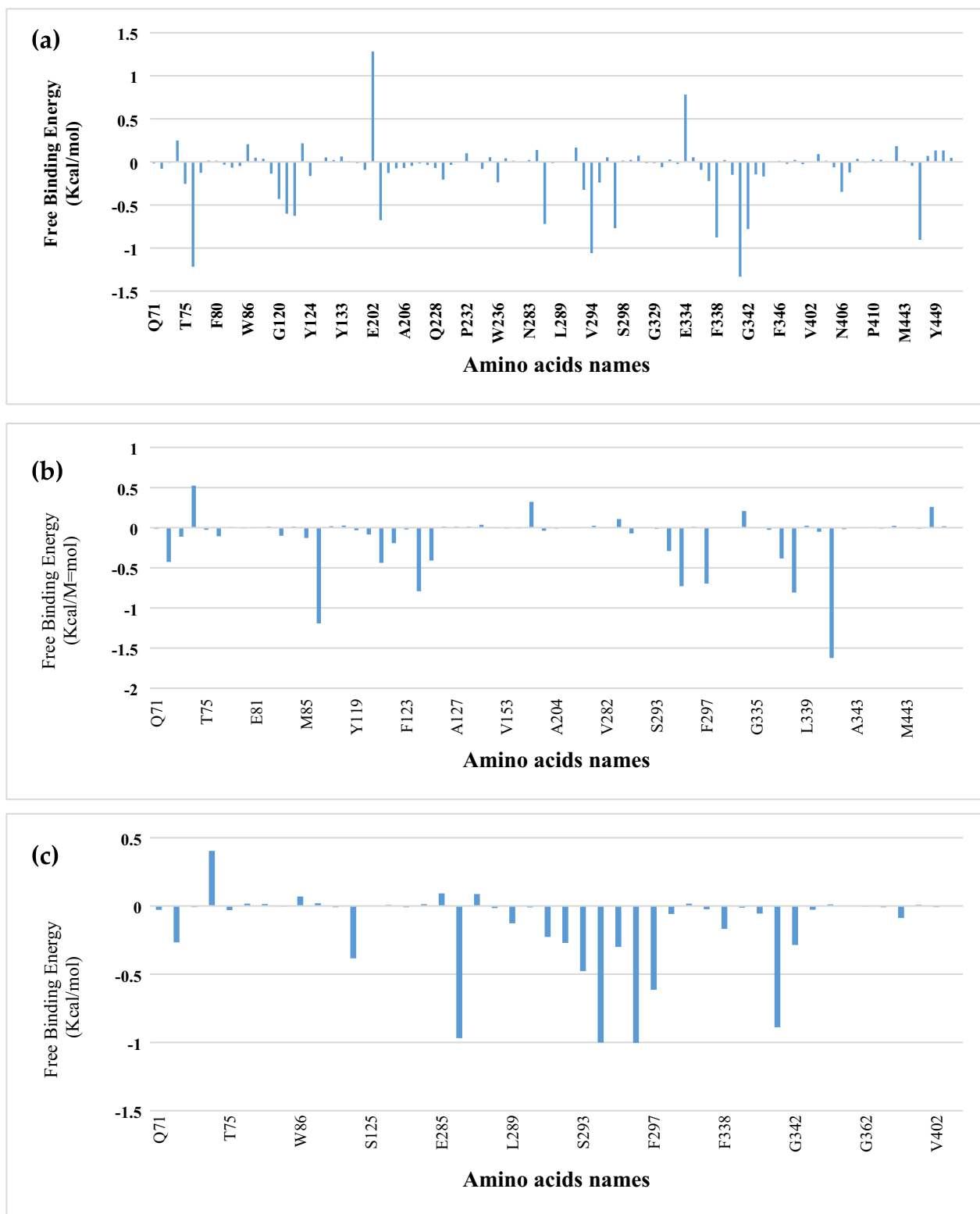
Fig. 14 MMPBSA free energy breakdown of residues within 10 Å of *h*AChE complexed with **a** donepezil, **b** dihydroactinidiolide, **c** thymol
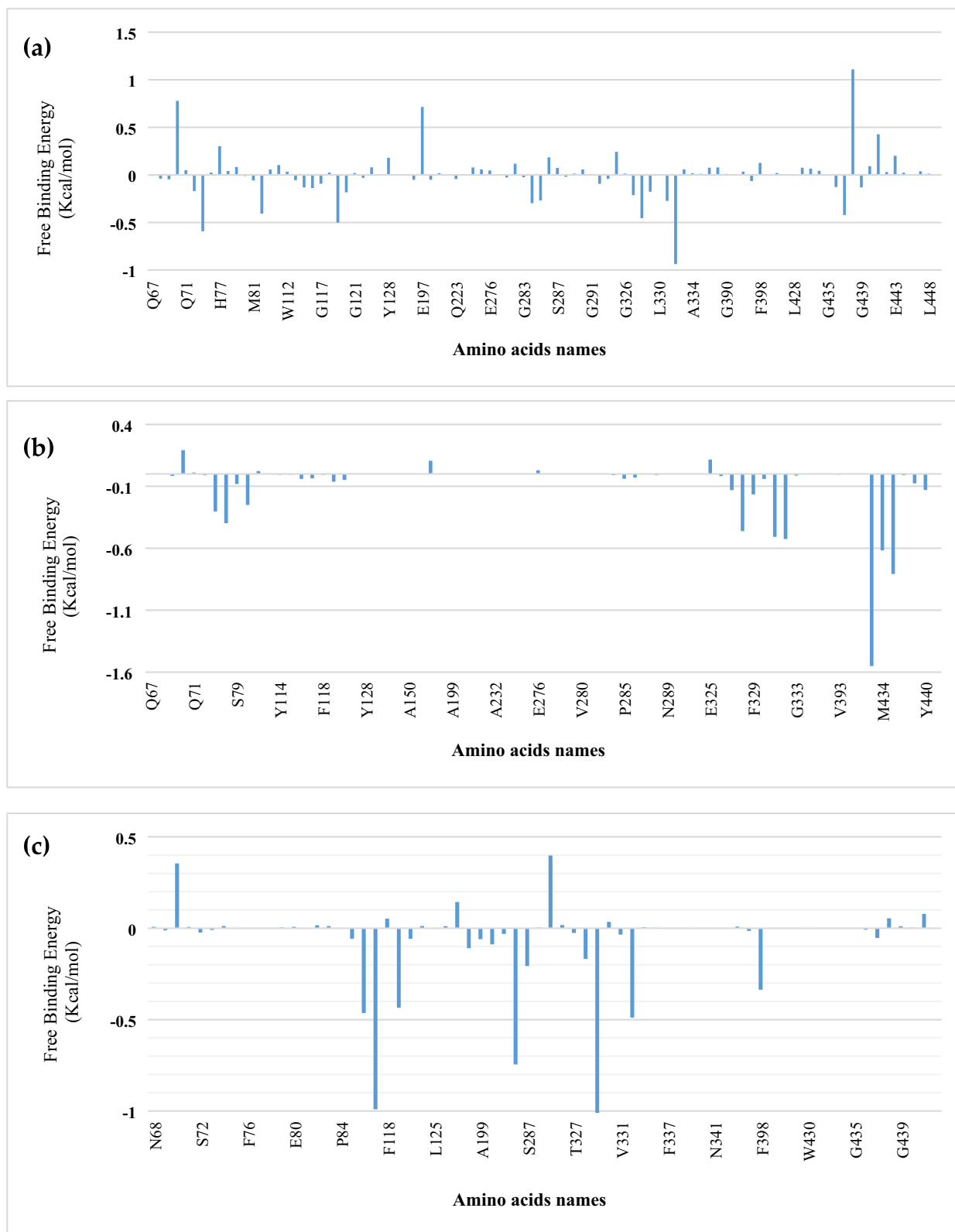
Fig. 15 MMPBSA free energy decomposition of residues within 10 Å of *h*BChE complexed with **a** propidium, **b** dihydroactinidiolide, **c** 1H-Indole-3-ethanamine
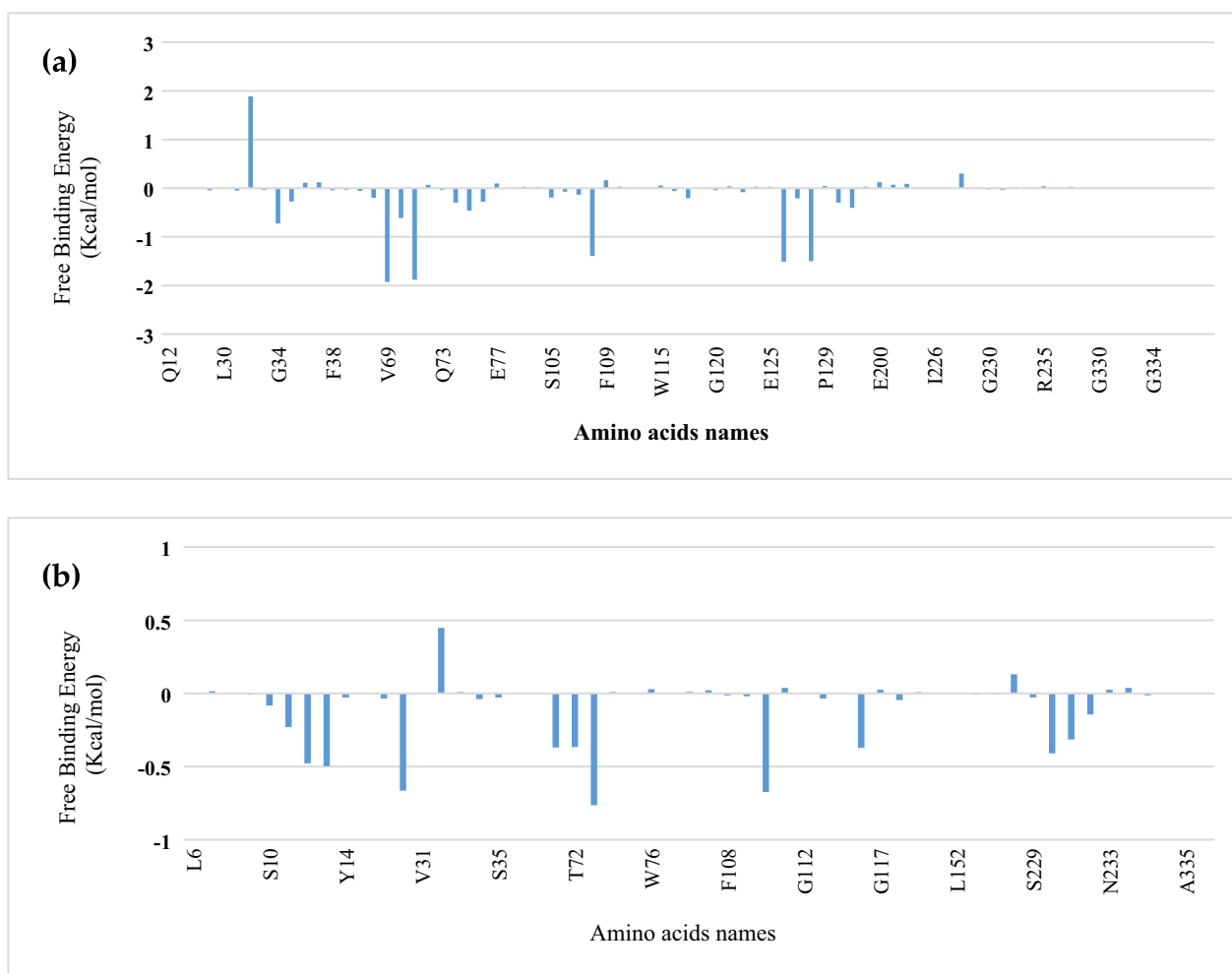
Fig. 16 MMPBSA free energy decomposition of residues within 10 Å of BACE-1 complexed with **a** Comp 1, **b** dihydroactinidiolide

reported the GC–MS chemical investigation of methanol extract of the leaf [62], ethanol extract from Soxhlet [63], methanol mixed with dimethyl sulfuroxide extract [64], freshly mild and air-dried [65]. This is the first study to report the GC–MS analysis of a *n*-hexane-partitioned fraction of the methanol extract of *Gl* leaf. The methodology used may have given rise to some identified compounds that have not been previously reported.

The advent of computational structure-based docking experiments has aided in the prediction of the best mode of interaction between two ligands and target receptors by employing binding mode analysis and scoring functions to evaluate noncovalent interactions [66]. An intensive interactive analysis was performed on the selected docked conformations of the phytochemicals and their respective targets by comparing the modes of interaction with the co-crystallized ligands and known inhibitors of these enzymes. The catalytic mechanism of these inhibitors in relation to important residues of the enzymes

and their implication in the inhibition of the activity of the enzymes has been documented [67–69]. The result from the initial docking analysis presented dihydroactinidiolide and 1H-Indole-3-ethanamine as having the highest multiple binding tendencies to hBChE, hBACE-1and hAβ fibrils proteins, while dihydroactinidiolide and thymol were the leading phytochemicals for hAChE. The lead phytochemicals were found housed in the thin, long, hydrophobic gorge of hAChE and hBChE in comparable binding patterns as donepezil [70], The lead phytochemicals interacted with the catalytic triad residues (Ser203, His447 and Glu334) and additional aromatic residues that project into the catalytic gorge [71], especially those of peripheral anionic site (P-site) residues that are positioned at the rim of the gorge and offer allosteric and inhibitors a binding site [69]. The lead phytochemicals also intermingled with the anionic choline-binding site residues (Trp86, Phe331 and Tyr334), among which
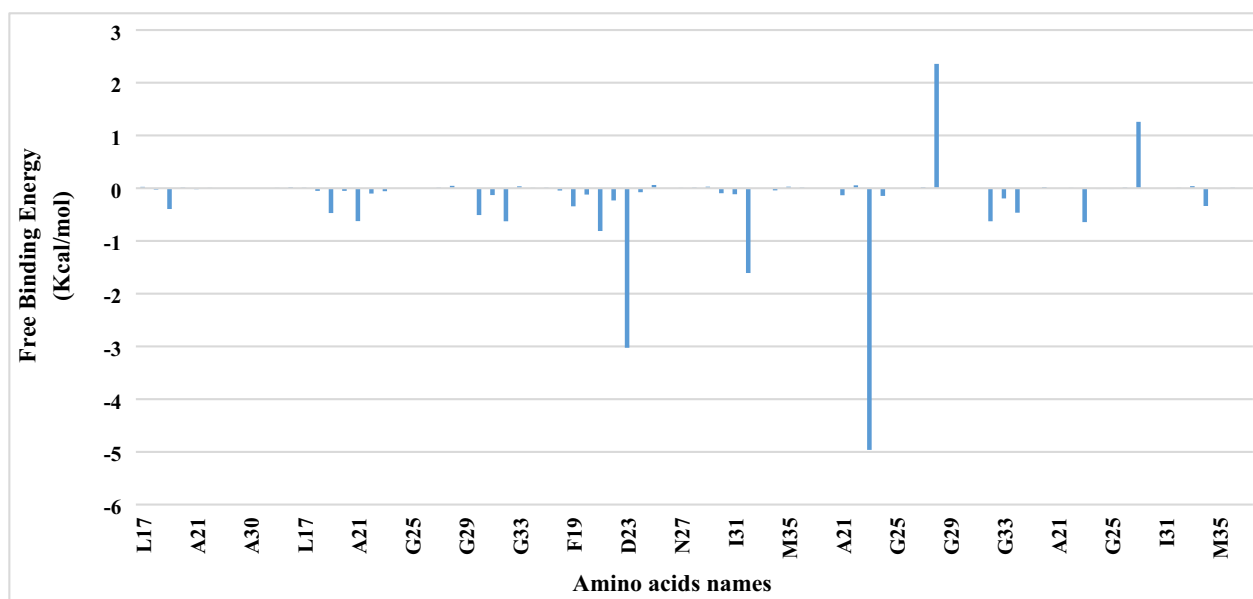
Fig. 17 MMPBSA free energy decomposition of residues within 10 Å of BACE-1 of 1H-Indole-3-ethanamine complexed to *h*Aβ fibrils

Trp86 and Try337 have been described as vital for the inhibition of the hAChE enzyme [67, 72].

The variation in the number of aromatic residues in the gorge of both *h*AChE and *h*BChE enzymes has been the major determinant of the difference in their ligand binding specificity; out of the total number of aromatic amino acid residues in *hAChE*, only 4 are present in the hydrophobic gorge of *h*BChE [73]. This may have informed the reason for selective binding of thymol to the *h*AChE.

Besides the strong binding tendencies to the cholinesterase enzymes, dihydroactinidiolide and 1H-Indole-3-ethanamine displayed comparative binding affinity for the active site residues of human beta-site APP cleaving enzyme1 (BACE1) to the reference co-crystallized inhibitor. Dihydroactinidiolide and 1H-Indole-3-ethanamine firmly accommodated in the binding cleft of the enzyme. Blocking the substrate binding cleft of the enzyme that contains the catalytic dyad (Asp32/Asp228) at the center of the cleft and is covered by a β-hairpin loop [74] has been reported as the best mode of inhibiting the catalytic activity of the enzyme [75]. Also, the lead phytocompounds interacted with the flip residues of the binding site of the enzyme, which has been stated to change the conformation of the entrance of the binding cleft, thereby blocking the substrate from accessing the cleft [76, 77]. Furthermore, dihydroactinidiolide and 1H-Indole-3-ethanamine interacted strongly with important residues of the Aβ fibrils. Previous studies have shown that the monomorphic Aβ comprises a residual structure with three discrete areas: the dominant hydrophobic region (Leu17–Ala21), the second hydrophobic region (Gly29–Met35) and the loop (Asp23–Lys28) region [78], which is bonded by inter-strand between remains that steady the structure [79]. Compounds that relate to these important amino acid remains that are located in the hydrophobic cores have been described to interrupt the accumulation of fibrils [80].

Ensemble-based molecular docking methodology, in which the test ligands are docked to several matches of the targeted enzymes, usually gotten from MD simulation, has recently been inaugurated as a better in-depth assessment of molecular docking [81]; interestingly, the outcome from the ensemble-based docking analysis collaborated with the initial docking analysis, further indicating that regardless of the change in conformation, the lead phytochemicals were able to interact with the active site amino acid residues. This result was further supported by the binding free energy computation and disintegration of binding free energy based on individual interacting amino acids. The interactions with catalytic residues that were detected in the static docking analysis were maintained in the dynamic docking computation. The structural integrity and flexibility of the lead phytochemicals from the docking analysis complexed with respective protein targets were likened to the apo protein make-up through the analysis of the MD simulation trajectories. The analysis of RMSD plots reveals the degree of departure of frames generated during simulation from the original structure; therefore, this analysis can be used to measure the stability of the various systems in the dynamic environment [82]. It was discerned that the binding of the lead compounds to hAChE, hBChE and

Table 7 In silico drug-likeness and ADMET parameters of the top two docked phytochemicals

	Dihydroactinidiolide	1H-Indole-3-ethanamine	Thymol
Molecular weight (g/mol)	180.24	160.22	150.22
Num. arom. Heavy atoms	0	9	6
Num. heavy atoms	13	12	11
Num. H-bond acceptors	2	1	1
Num. rotatable bonds	0	2	1
Hydrogen bond donor	0	2	1
cLogP	2.29	1.54	2.32
Molar refractivity	51.35	50.78	48.01
TPSA (Å^2)	26.30	41.81	20.23
Drug-likeness			
Lipinski	Yes	Yes	Yes
Veber	Yes	Yes	Yes
Ghose	Yes	Yes	No (MW < 160)
Egan	Yes	Yes	Yes
Bioavailability score	0.55	0.55	0.17
Absorption (probability)			
(b) Admet SAR			
HIA	HIA + (1.0)	HIA + (0.767)	HIA + (0.805)
Blood–brain barrier	BBB + (0.9545)	BBB + (0.939)	BBB + (0.0568)
P-glycoprotein substrate	Negative (0.5333)	Negative (0.279)	Negative (0. 037)
Caco-2 permeability Cm/s	Caco2 + (0.6787)	Caco2 + (0.066)	Caco2 + (0.576)
Distribution (probability)			
PPB %	64.639	53.854	80.06
Metabolism (probability)			
CYP450 1A2 inhibitor	Negative (0.563)	Positive (0.968)	Positive (0.799)
CYP450 1A2 substrate	Negative (0.408)	Positive (0.556)	Positive (0.566)
CYP450 3A4 inhibitor	Negative (0.866)	Negative (0.205)	Negative (0.118)
CYP450 2C9 inhibitor	Negative (0.900)	Negative (0.049)	Negative (0.337)
CYP450 2C9 substrate	Negative (0.8401)	Negative (0.607)	Negative (0.643)
CYP450 2C19 inhibitor	Positive (0.5211)	Negative (0.122)	Negative (0.735)
CYP450 2C19 substrate	Negative (0.452)	Positive (0.452)	Positive (0.491)
CYP450 2D6 inhibitor	Negative (0.922)	Negative (0.9022)	Negative (0.386)
CYP450 2D6 substrate	Negative (0.922)	Negative (0.505)	Positive (0.72)
Elimination			
$T_{1/2}$ (half life time)	0.013 h	1.216 h	1.313 h
CL (clearance rate) mL/min/kg	13.57	2.29	2.235
Toxicity			
hERG blockers	Negative (0.235)	Negative (0.222)	Negative (0.899)
AMES	Negative (0.937)	Negative (0.933)	Negative (0.928)
Carcinogen	Negative (0.918)	Negative (0.925)	Negative (0.719)
SkinSen	Negative (0.713)	Negative (0.236)	Negative (0.235)
LD$_{50}$ (LD$_{50}$ of acute toxicity)	1.948 -log mol/kg (2031.74 mg/kg)	2.497 -log mol/kg (510.172 mg/kg)	2.705 -log mol/kg (507.65 mg/kg)

ADMET absorption, distribution, metabolism, elimination, and toxicity, *BBB* blood–brain barrier, *GI*: *CYP* cytochrome P450, *P-gp* permeability glycoprotein, *hERG* human Ether-à-go-go-Related Gene, Gastro-intestinal, *H-HT* human hepatotoxicity AMES, *HIA* human intestinal absorption, *DILI* drug-induced liver injury, *VD* volume distribution, Ames mutagenicity, *PPB* plasma protein binding
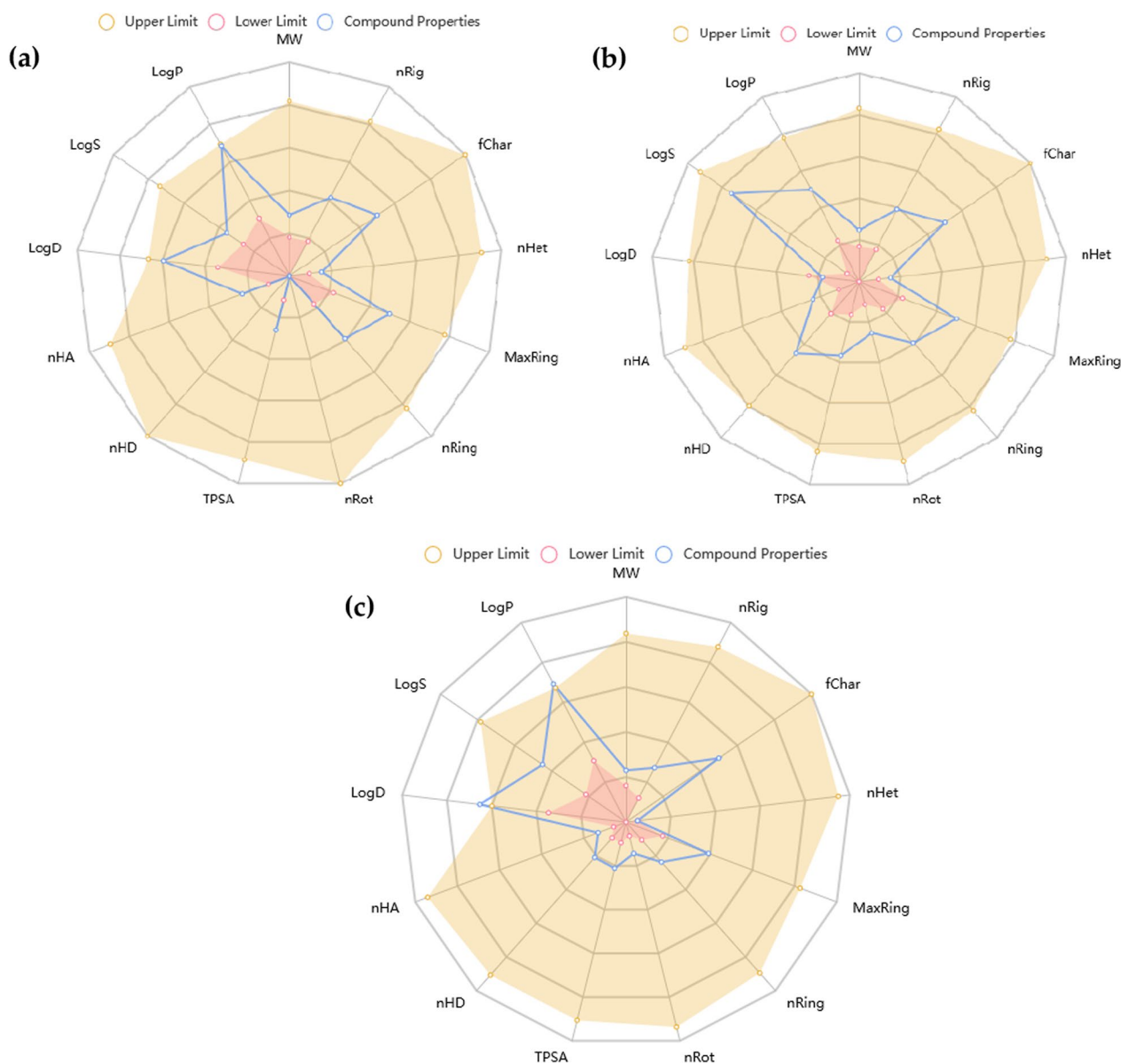
Fig. 18 The radar plot of in silico physicochemical of top docked phytochemical from the docking analysis **a** dihydroactinidiolide, **b** 1H-Indole-3-ethanamine, **c** thymol. The radar plot shows the physicochemical properties of the phytochemical (in blue) and the reference optimal scope (in red and yellow)

BACE-1 caused a reduction in the mean RMSD when likened to the free protein, showing that the binding of the lead compound enhanced the strength of the system [82]. But the binding of 1H-Indole-3-ethanamine to the hAβ fibril increased the mean RMSD value coupled with the large fluctuations that were observed between 10 and 80 ns during the period of simulation, further signifying a major restructuring of the structures and a disruption or destabilization of the assembled Aβ fibrils [57]. Furthermore, the flexibility of the individual remains of the protein system was measured from the RMSF plots and mean values. During the period of simulation, the passage of a subset of atoms, in relation to the entire structure over the total simulation, can be measured from the RMSF plots. Also, there are spikes that appear at the C and N terminal ends of the proteins as a result of the terminal motions [82]. The various adaptations in flexibility lie primarily in the areas or residues of the order that impact the conformational steadiness of the Aβ fibrils complex [83]. The reduction in RMSF values

Gyebi *et al. Future Journal of Pharmaceutical Sciences*   (2023) 9:84

Page 29 of 33

in the complexes compared to the freed protein shows more compressed complexes, unlike the 1H-Indole-3-ethanamine that increased the fluctuation around residue numbers 18–21 and the corresponding mean RMSF value, signifying a change in conformation with hAβ fibrils. The results from the RoG, SASA and number of hydrogen atoms show that the integrity and compactness of the hAChE, hBChE and BACE-1 structures were not compromised by the binding of the lead phytochemicals [82, 83]. The result obtained from the four drugability filtering analyses shows that the lead phytocompounds have favorable pharmacokinetic properties with good bioavailability [84, 85]. The result obtained from the four drugability filtering analysis shows that the lead phytocompounds have favorable pharmacokinetic properties with good bioavailability [86–89]. Among the various in silico predictive molecular descriptors for toxicity that were examined, the hERG channel plays a vital role in the repolarization and cessation stages of action capacity, especially in cardiac cells. Inhibitors of the hERG outlet have been reported to cause cardiotoxicity [90]. The lead phytochemicals (dihydroactinidiolide, 1H-Indole-3-ethanaminea and thymol) did not present the tendencies of being hERG outlet blockers, signifying that they may not trigger hERG channel-related cardiotoxicity [90, 91]. This may have been responsible for their predicted nonhuman hepatotoxicity [92]. Also, using the numerous cytochrome P450 descriptors, the effect of the lead compounds on phase I drug metabolism was investigated. The lead phytochemicals established less inhibitory ability for the diverse cytochrome P450; hence, they may not adversely affect phase I drug metabolism to a large extent [91]. The lead phytochemicals were further predicted to have good human intestinal absorption and bioavailability, specifying that they may be administered through the oral route [93]. The lead phytocompounds did not present AMES mutagenicity, drug-induced liver injury or carcinogenicity; hence, they may not cause cellular or genotoxicity [94]. The BBB is known as a barricade shielding the brain via a 'physical' barricade and a 'biochemical' blockade that is comprised of dynamic efflux and several enzymatic activities [95] that serves as an essential fence between the systemic circulation and CNS. This has been one of the greatest challenges in CNS drug delivery [96]. Among the numerous molecular descriptors that were studied in silico, the lead phytochemicals presented the tendencies of crossing the blood–brain barrier (BBB) which help to specify that the compounds can get to the brain or CNS where they exercise their neuroprotective role [97]. The multi-target inhibitory potential of the lead phytochemicals against hAChE, hBChE and BACE-1 and the fibril-disruptive tendencies, coupled with the potential to cross the BBB, show hopeful drug candidates that

can be useful for managing or treating neurodegenerative diseases such as AD.

Comparing the results obtained from this study, it is interesting to observe that in a recent and related study on *Trachyandra laxa* (N.E.Br.), a tumbleweed, dihydroactinidiolide was suggested to be one of the neuroprotective constituents of the plant [98]. Dihydroactinidiolide, an α,β-unsaturated lactone that is usually found in nature as a yield of carotenoids degradation [99] has been previously reported to inhibit AChE with an IC50 34.03 nM, with good DPPH and (.NO) hunting activity, coupled with the ability to significantly prevent amyloid β25–35 self-accumulation and promote its separation [100]. In the same vein, 1H-Indole-3-ethanamine is also known as tryptamine, and several derivatives have been described to have cholinesterase inhibitory activities with neuroprotective and β-secretase inhibitory and β-amyloid (Aβ) aggregation activities [101–105]. Also, thymol has been reported to have in vitro acetylcholinesterase [106–108]. In a similar study design as our present study, which involves in vitro acetylcholinesterase inhibitory activity, GC–MS chemical profiling and in silico studies, thymol was identified as one of the cholinergic inhibitors in *Lippia thymoides* [109].

Conclusion

Herein, we employed in vitro anti-cholinergic and monoamine oxidase inhibitory activities, GC–MS chemical profiling and in silico approaches to identify potential neuroprotective phytochemicals from the *n*-hexane solvent partition fraction of methanol extracts of *Gongronema latifolium*. The solvent fraction demonstrated concentration-dependent cholinergic inhibitory activities. Molecular docking analysis of the GC–MS identified compounds identified dihydroactinidiolide, 1H-Indole-3-ethanamine with multi-target inhibitory tendencies against hAChE, hBChE and BACE-1 in addition to fibril-disruptive tendencies. Both ensemble-docking and binding free energy based on MMPBSA computation confirmed the strong interaction of the lead phytochemicals with catalytic residues of the target proteins. The ligand–protein complexes were stable during the period of MD simulation. The favorable drug-likeness and ADMET properties, in addition to the capability to cross the BBB, suggest these phytocompounds as promising drug candidates that can be useful for managing or treating neurodegenerative diseases such as AD. The lead phytochemicals, in part or in synergy, may be responsible for the neuroprotective activities of *Gongronema latifolium* leaf. These complexes can serve as potential lead compounds for the development of drugs to counter neurodegenerative

Gyebi *et al. Future Journal of Pharmaceutical Sciences*   (2023) 9:84

Page 30 of 33

diseases; they are therefore recommended for further studies (Additional file 1).

Abbreviations

NDDs	Neurodegenerative disorders
AChE	Acetylcholinesterase
BChE	Butyrylcholinesterase
MAO	Monoamine oxidase
*h*AChE	Human acetylcholinesterase
*h*BChE	Human butyrylcholinesterase
hBACE1	Human β-secretase enzyme 1
hAβ	Human amyloid beta Aβ
AD	Alzheimer's disease
PD	Parkinson's disease
HF	*n*-Hexane solvent partition fraction of methanol extract of *Gongronema latifolium* leaf
GC–MS	Gas chromatography mass spectrometry
EBD	Ensemble-based docking
MDs	Molecular dynamics simulation
LPs	Lead phytochemicals
BACE1	β-Secretase enzyme
BFG	Binding free energy
ADMET	Adsorption, distribution, metabolism, excretion and toxicity

Supplementary Information

The online version contains supplementary material available at https://doi.org/10.1186/s43094-023-00536-7.

> **Additional file 1: Fig. S1.** Histogram of clusters from the group analysis of the MDS trajectories of 4ey7; **Fig. S2.** Histogram of clusters from the cluster investigation of the MDS trajectories of 6ep4; **Fig. S3.** Histogram of clusters from the cluster examination of the MDS trajectories of 5i3v.

Availability of data and materials

The data sets used and analyzed during the current study are available from the corresponding author upon reasonable request.

Declarations

Ethics approval and consent to participate

The authors did not use human or animal subject. Appropriate approval to research on the studied plant was duly granted by the University of Ilorin Ethical Review Committee with the Approval Number: UERC/ASN/2018/1526.

Consent for publication

The authors declare no conflict of interest.

Competing interests

The authors declare that they have no competing interests.

Author details

[1]Department of Biochemistry, Faculty of Science and Technology, Bingham University, Karu, Nasarawa, Nigeria. [2]Natural Products and Structural (Bio-Chem)-Informatics Research Laboratory (NpsBC-Rl), Bingham University, Karu, Nasarawa, Nigeria. [3]Nutritional and Industrial Biochemistry Unit, Department of Biochemistry, Faculty of Basis Medical Sciences, College of Medicine, University of Ibadan, Ibadan, Nigeria. [4]Department of Human Anatomy, Faculty of Basic Medical Sciences, Bingham University, Karu, Nasarawa, Nigeria. [5]Department of Biophysics, Faculty of Sciences, Cairo University, Giza, Egypt. [6]Department of Pharmacology and Therapeutics, Faculty of Basic Medical Sciences, University of Ilorin, Ilorin, Nigeria. [7]Department of Biochemistry, Faculty of Computing and Applied Sciences, Baze University, Abuja, Nigeria. [8]Department of Biological Sciences, KolaDaisi University, Ibadan, Nigeria. [9]Department of Pharmaceutical Sciences, College of Pharmacy, Princess Nourah Bint Abdulrahman University, P.O. Box 84428, 11671 Riyadh, Saudi Arabia. [10]Department of Pharmacology and Therapeutics, Faculty of Veterinary Medicine, Damanhour University, Damanhour 22511, AlBeheira, Egypt.

References

1. Behl T, Kaur D, Sehgal A, Singh S, Sharma N, Zengin G, Andronie-Cioara FL, Toma MM, Bungau S, Bumbu AG (2021) Role of monoamine oxidase activity in Alzheimer's disease: an insight into the therapeutic potential of inhibitors. Molecules 26(12):3724
2. Mubangizi V, Maling S, Obua C, Tsai AC (2020) Prevalence and correlates of Alzheimer's disease and related dementias in rural Uganda: cross-sectional, population-based study. BMC Geriatr 20(1):1–7
3. Ojagbemi A, Okekunle AP, Babatunde O (2021) Dominant and modifiable risk factors for dementia in sub-Saharan Africa: a systematic review and meta-analysis. Front Neurol 12:627761
4. Li X, Feng X, Sun X, Hou N, Han F, Liu Y (2022) Global, regional, and national burden of Alzheimer's disease and other dementias, 1990–2019. Front Aging Neurosci 14:937486
5. Bozoki A, Giordani B, Heidebrink JL, Berent S, Foster NL (2001) Mild cognitive impairments predict dementia in nondemented elderly patients with memory loss. Arch Neurol 58(3):411–416
6. Nichols E, Steinmetz JD, Vollset SE, Fukutaki K, Chalek J, Abd-Allah F, Abdoli A, Abualhasan A, Abu-Gharbieh E, Akram TT (2022) Estimation of the global prevalence of dementia in 2019 and forecasted prevalence in 2050: an analysis for the Global Burden of Disease Study 2019. Lancet Public Health 7(2):e105–e125
7. Bar-Am O, Amit T, Kupershmidt L, Aluf Y, Mechlovich D, Kabha H, Danovitch L, Zurawski VR, Youdim MB, Weinreb O (2015) Neuroprotective and neurorestorative activities of a novel iron chelator-brain selective monoamine oxidase-A/monoamine oxidase-B inhibitor in animal models of Parkinson's disease and aging. Neurobiol Aging 36(3):1529–1542
8. Hampel H, Mesulam M-M, Cuello AC, Farlow MR, Giacobini E, Grossberg GT, Khachaturian AS, Vergallo A, Cavedo E, Snyder PJ (2018) The cholinergic system in the pathophysiology and treatment of Alzheimer's disease. Brain 141(7):1917–1933
9. Humpel C (2011) Chronic mild cerebrovascular dysfunction as a cause for Alzheimer's disease? Exp Gerontol 46(4):225–232
10. Klafki H-W, Staufenbiel M, Kornhuber J, Wiltfang J (2006) Therapeutic approaches to Alzheimer's disease. Brain 129(11):2840–2855
11. Jellinger KA, Korczyn AD (2018) Are dementia with Lewy bodies and Parkinson's disease dementia the same disease? BMC Med 16(1):1–16
12. Surmeier DJ (2018) Determinants of dopaminergic neuron loss in Parkinson's disease. FEBS J 285(19):3657–3668
13. Bellucci A, Navarria L, Zaltieri M, Falarti E, Bodei S, Sigala S, Battistin L, Spillantini M, Missale C, Spano P (2011) Induction of the unfolded protein response by α-synuclein in experimental models of Parkinson's disease. J Neurochem 116(4):588–605
14. Hampel H, Lista S, Vanmechelen E, Zetterberg H, Giorgi FS, Galgani A, Blennow K, Caraci F, Das B, Yan R (2020) β-Secretase1 biological markers for Alzheimer's disease: state-of-art of validation and qualification. Alzheimer's Res Ther 12(1):1–14

Gyebi *et al. Future Journal of Pharmaceutical Sciences*   (2023) 9:84

Page 31 of 33

15. Hampel H, Vassar R, De Strooper B, Hardy J, Willem M, Singh N, Zhou J, Yan R, Vanmechelen E, De Vos A (2021) The β-secretase BACE1 in Alzheimer's disease. Biol Psychiat 89(8):745–756

16. Carocci A, Catalano A, Sinicropi MS, Genchi G (2018) Oxidative stress and neurodegeneration: the involvement of iron. Biometals 31(5):715–735

17. Ramli NZ, Yahaya MF, Tooyama I, Damanhuri HA (2020) A mechanistic evaluation of antioxidant nutraceuticals on their potential against age-associated neurodegenerative diseases. Antioxidants 9(10):1019

18. Ward RJ, Dexter DT, Crichton RR (2012) Chelating agents for neurodegenerative diseases. Curr Med Chem 19(17):2760–2772

19. D'Onofrio G, Nabavi SM, Sancarlo D, Greco A, Pieretti S (2021) *Crocus sativus* L. (Saffron) in Alzheimer's disease treatment: bioactive effects on cognitive impairment. Curr Neuropharmacol 19(9):1606

20. Hannan MA, Rahman MA, Sohag AAM, Uddin MJ, Dash R, Sikder MH, Rahman MS, Timalsina B, Munni YA, Sarker PP (2021) Black cumin (*Nigella sativa* L.): a comprehensive review on phytochemistry, health benefits, molecular pharmacology, and safety. Nutrients 13(6):1784

21. Mima Y, Izumo N, Chen J-R, Yang S-C, Furukawa M, Watanabe Y (2020) Effects of *Coriandrum sativum* seed extract on aging-induced memory impairment in Samp8 mice. Nutrients 12(2):455

22. Aloni PD, Nayak AR, Chaurasia SR, Deopujari JY, Chourasia C, Purohit HJ, Taori GM, Daginawala HF, Kashyap RS (2016) Effect of Fagonia arabica on thrombin induced release of t-PA and complex of PAI-1 tPA in cultured HUVE cells. J Tradit Complement Med 6(3):219–223

23. Patil SM, Ramu R, Shirahatti PS, Shivamallu C, Amachawadi RG (2021) A systematic review on ethnopharmacology, phytochemistry and pharmacological aspects of *Thymus vulgaris* Linn. Heliyon 7(5):e07054

24. Eskandari-Roozbahani N, Shomali T, Taherianfard M (2019) Neuroprotective effect of *Zataria multiflora* essential oil on rats with Alzheimer disease: a mechanistic study. Basic Clin Neurosci 10(1):85

25. Ojo OA, Okesola MA, Ekakitie LI, Ajiboye BO, Oyinloye BE, Agboinghale PE, Onikanni AS (2020) *Gongronema latifolium* Benth. leaf extract attenuates diabetes-induced neuropathy via inhibition of cognitive, oxidative stress and inflammatory response. J Sci Food Agric 100(12):4504–4511

26. Ogunyemi OM, Gyebi GA, Ibrahim IM, Esan AM, Olaiya CO, Soliman MM, Batiha GE-S (2022) Identification of promising multi-targeting inhibitors of obesity from *Vernonia amygdalina* through computational analysis. Mol Divers 27:1–25

27. Ojo OA, Ojo AB, Okolie C, Nwakama M-AC, Iyobhebhe M, Evbuomwan IO, Nwonuma CO, Maimako RF, Adegboyega AE, Taiwo OA (2021) Deciphering the interactions of bioactive compounds in selected traditional medicinal plants against Alzheimer's diseases via pharmacophore modeling, auto-QSAR, and molecular docking approaches. Molecules 26(7):1996

28. Oyinloye BE, Iwaloye O, Ajiboye BO (2021) Polypharmacology of *Gongronema latifolium* leaf secondary metabolites against protein kinases implicated in Parkinson's disease and Alzheimer's disease. Sci Afr 12:e00826

29. Morebise O, Fafunso MA, Makinde JM, Olajide OA, Awe E (2002) Antiinflammatory property of the leaves of *Gongronema latifolium*. Phytother Res 16(S1):75–77

30. Nwanna E, Oyeleye S, Ogunsuyi O, Oboh G, Boligon A, Athayde M (2016) In vitro neuroprotective properties of some commonly consumed green leafy vegetables in Southern Nigeria. NFS J 2:19–24

31. Ogundipe O, Moody J, Akinyemi T, Raman A (2003) Hypoglycemic potentials of methanolic extracts of selected plant foods in alloxanized mice. Plant Foods Hum Nutr 58(3):1–7

32. Harbone J (1980) Phytochemical analysis: a guide to modern techniques of plant analysis. Chapman & Hall, New York

33. Gyebi GA, Adebayo JO, Olorundare OE, Pardede A, Ninomiya M, Saheed AO, Babatunde AS, Koketsu M (2018) Iloneoside: a cytotoxic ditigloylated pregnane glycoside from the leaves of *Gongronema latifolium* Benth. Nat Prod Res 32(24):2882–2886

34. Ellman GL, Courtney KD, Andres V Jr, Featherstone RM (1961) A new and rapid colorimetric determination of acetylcholinesterase activity. Biochem Pharmacol 7(2):88–95

35. Perry NS, Houghton PJ, Theobald A, Jenner P, Perry EK (2000) In-vitro inhibition of human erythrocyte acetylcholinesterase by *Salvia lavandulaefolia* essential oil and constituent terpenes. J Pharm Pharmacol 52(7):895–902

36. Turski W, Turska E, Gross-Bellard M (1972) Modification of the spectrophotometric method of the determination of monoamine oxidase. Enzyme 14:211–220

37. Green A, Haughton TM (1961) A colorimetric method for the estimation of monoamine oxidase. Biochem J 78(1):172–175

38. Morris GM, Huey R, Lindstrom W, Sanner MF, Belew RK, Goodsell DS, Olson AJ (2009) AutoDock4 and AutoDockTools4: automated docking with selective receptor flexibility. J Comput Chem 30(16):2785–2791

39. O'Boyle NM, Banck M, James CA, Morley C, Vandermeersch T, Hutchison GR (2011) Open Babel: an open chemical toolbox. J Cheminform. https://doi.org/10.1186/1758-2946-3-33

40. Trott O, Olson AJ (2010) AutoDock Vina: improving the speed and accuracy of docking with a new scoring function, efficient optimization, and multithreading. J Comput Chem 31(2):455–461. https://doi.org/10.1002/jcc.21334

41. Abraham MJ, Murtola T, Schulz R, Páll S, Smith JC, Hess B, Lindahl E (2015) GROMACS: high performance molecular simulations through multi-level parallelism from laptops to supercomputers. SoftwareX 1:19–25

42. Bekker H, Berendsen H, Dijkstra E, Achterop S, Vondrumen R, Vanderspoel D, Sijbers A, Keegstra H, Renardus M (eds) (1993) Gromacs-a parallel computer for molecular-dynamics simulations. In: 4th international conference on computational physics (PC 92). World Scientific Publishing

43. Oostenbrink C, Villa A, Mark AE, Van Gunsteren WF (2004) A biomolecular force field based on the free enthalpy of hydration and solvation: the GROMOS force-field parameter sets 53A5 and 53A6. J Comput Chem 25(13):1656–1676

44. Schüttelkopf AW, Van Aalten DM (2004) PRODRG: a tool for high-throughput crystallography of protein–ligand complexes. Acta Crystallogr D Biol Crystallogr 60(8):1355–1363

45. Humphrey W, Dalke A, Schulten K (1996) VMD: visual molecular dynamics. J Mol Graph 14(1):33–38

46. Tubiana T, Carvaillo J-C, Boulard Y, Bressanelli S (2018) TTClust: a versatile molecular simulation trajectory clustering program with graphical summaries. J Chem Inf Model 58(11):2178–2182

47. Hanwell MD, Curtis DE, Lonie DC, Vandermeersch T, Zurek E, Hutchison GR (2012) Avogadro: an advanced semantic chemical editor, visualization, and analysis platform. J Cheminform 4(1):17. https://doi.org/10.1186/1758-2946-4-17

48. Fliege J, Svaiter BF (2000) Steepest descent methods for multicriteria optimization. Math Methods Oper Res 51(3):479–494

49. Rappe AK, Casewit CJ, Colwell KS, Goddard WA, Skiff WM (1992) UFF, a full periodic table force field for molecular mechanics and molecular dynamics simulations. J Am Chem Soc 114(25):10024–10035. https://doi.org/10.1021/ja00051a040

50. Salentin S, Schreiber S, Haupt V, Adasme M, Schroeder M (2015) PLIP: fully automated protein-ligand interaction profiler. Nucleic Acids Res. https://doi.org/10.1093/nar/gkv315

51. Valdés-Tresanco MS, Valdés-Tresanco ME, Valiente PA, Moreno E (2021) gmx_MMPBSA: a new tool to perform end-state free energy calculations with GROMACS. J Chem Theory Comput 17(10):6281–6291

52. Miller BR III, McGee TD Jr, Swails JM, Homeyer N, Gohlke H, Roitberg AE (2012) MMPBSA. py: an efficient program for end-state free energy calculations. J Chem Theory Comput 8(9):3314–3321

53. Xue W, Yang F, Wang P, Zheng G, Chen Y, Yao X, Zhu F (2018) What contributes to serotonin–norepinephrine reuptake inhibitors' dual-targeting mechanism? The key role of transmembrane domain 6 in human serotonin and norepinephrine transporters revealed by molecular dynamics simulation. ACS Chem Neurosci 9(5):1128–1140

54. Tuccinardi T (2021) What is the current value of MM/PBSA and MM/GBSA methods in drug discovery? Taylor & Francis, London, pp 1233–1237

55. Ali-Shtayeh MS, Jamous RM, Zaitoun SYA, Qasem IB (2014) In-vitro screening of acetylcholinesterase inhibitory activity of extracts from

Gyebi *et al. Future Journal of Pharmaceutical Sciences*   (2023) 9:84

Page 32 of 33

Palestinian indigenous flora in relation to the treatment of Alzheimer's disease. Funct Foods Health Dis 4(9):381–400

56. Mukherjee S, Balius TE, Rizzo RC (2010) Docking validation resources: protein family and ligand flexibility experiments. J Chem Inf Model 50(11):1986–2000

57. Adewole KE, Gyebi GA, Ibrahim IM (2021) Amyloid β fibrils disruption by kolaviron: molecular docking and extended molecular dynamics simulation studies. Comput Biol Chem 94:107557

58. Xiong G, Wu Z, Yi J, Fu L, Yang Z, Hsieh C, Yin M, Zeng X, Wu C, Lu A (2021) ADMETlab 2.0: an integrated online platform for accurate and comprehensive predictions of ADMET properties. Nucleic Acids Res 49(W1):W5–W14

59. Nwanna EE, Adebayo AA, Oboh G, Ogunsuyi OB, Ademosun AO (2019) Modulatory effects of alkaloid extract from *Gongronema latifolium* (Utazi) and *Lasianthera africana* (Editan) on activities of enzymes relevant to neurodegeneration. J Diet Suppl 16(1):27–39

60. Ademosun AO, Oboh G (2014) Comparison of the inhibition of mono-amine oxidase and butyrylcholinesterase activities by infusions from green tea and some citrus peels. Int J Alzheimer's Dis. https://doi.org/10.1155/2014/586407

61. Ballard C (2002) Advances in the treatment of Alzheimer's disease: benefits of dual cholinesterase inhibition. Eur Neurol 47(1):64–70

62. Ali F, Ibiam U (2014) Phytochemical studies and GC–MS analysis of *Gongronema latifolium* and *Piper guineense*. Int J Innov Res Dev 3(9):108–115

63. Al-Hindi B, Yusoff NA, Atangwho IJ, Ahmad M, Asmawi MZ, Yam MF (2016) A soxhlet extract of *Gongronema latifolium* retains moderate blood glucose lowering effect and produces structural recovery in the pancreas of STZ-induced diabetic rats. Med Sci 4(2):9

64. Willie P, Uyoh EA, Aikpokpodion PO (2021) Gas chromatography–mass spectrometry (GC–MS) assay of bio-active compounds and phyto-chemical analyses in three species of apocynaceae. Pharmacogn J 13(2):383–392

65. Okafor V (2016) Spectroscopic methods for evaluation of hop extracts and extract from *Gongronema latifolium* as substitute in the Nigerian beer industry. Int J Adv Res 4(12):2499–2504

66. Trezza A, Iovinelli D, Santucci A, Prischi F, Spiga O (2020) An integrated drug repurposing strategy for the rapid identification of potential SARS-CoV-2 viral inhibitors. Sci Rep 10(1):1–8

67. Harel M, Schalk I, Ehret-Sabatier L, Bouet F, Goeldner M, Hirth C, Axelsen P, Silman I, Sussman J (1993) Quaternary ligand binding to aromatic residues in the active-site gorge of acetylcholinesterase. Proc Natl Acad Sci 90(19):9031–9035

68. Silman I, Harel M, Axelsen P, Raves M, Sussman JL (1994) Three-dimensional structures of acetylcholinesterase and of its complexes with anticholinesterase agents. Biochem Soc Trans 22(3):745–749

69. Sussman JL, Harel M, Frolow F, Oefner C, Goldman A, Toker L, Silman I (1991) Atomic structure of acetylcholinesterase from *Torpedo californica*: a prototypic acetylcholine-binding protein. Science 253(5022):872–879

70. Hines M, Blum J (1979) Bend propagation in flagella. II. Incorporation of dynein cross-bridge kinetics into the equations of motion. Biophys J 25(3):421–441

71. Ordentlich A, Barak D, Kronman C, Flashner Y, Leitner M, Segall Y, Ariel N, Cohen S, Velan B, Shafferman A (1993) Dissection of the human acetylcholinesterase active center determinants of substrate specificity. Identification of residues constituting the anionic site, the hydrophobic site, and the acyl pocket. J Biol Chem 268(23):17083–17095

72. Ashani Y, Grunwald J, Kronman C, Velan B, Shafferman A (1994) Role of tyrosine 337 in the binding of huperzine A to the active site of human acetylcholinesterase. Mol Pharmacol 45(3):555–560

73. Darvesh S, Hopkins DA, Geula C (2003) Neurobiology of butyrylcholinesterase. Nat Rev Neurosci 4(2):131–138. https://doi.org/10.1038/nrn1035

74. Xu Y, Mj Li, Greenblatt H, Chen W, Paz A, Dym O, Peleg Y, Chen T, Shen X, He J (2012) Flexibility of the flap in the active site of BACE1 as revealed by crystal structures and molecular dynamics simulations. Acta Crystallogr D Biol Crystallogr 68(1):13–25

75. Mouchlis VD, Melagraki G, Zacharia LC, Afantitis A (2020) Computer-aided drug design of β-secretase, γ-secretase and anti-tau inhibitors for the discovery of novel Alzheimer's therapeutics. Int J Mol Sci 21(3):703

76. Gupta S, Parihar D, Shah M, Yadav S, Managori H, Bhowmick S, Patil PC, Alissa SA, Wabaidur SM, Islam MA (2020) Computational screening of promising beta-secretase 1 inhibitors through multi-step molecular docking and molecular dynamics simulations-pharmacoinformatics approach. J Mol Struct 1205:127660

77. Kumar A, Roy S, Tripathi S, Sharma A (2016) Molecular docking based virtual screening of natural compounds as potential BACE1 inhibitors: 3D QSAR pharmacophore mapping and molecular dynamics analysis. J Biomol Struct Dyn 34(2):239–249

78. Boopathi S, Kolandaivel P (2014) Role of zinc and copper metal ions in amyloid β-peptides Aβ 1–40 and Aβ 1–42 aggregation. RSC Adv 4(73):38951–38965

79. Tarus B, Straub JE, Thirumalai D (2006) Dynamics of Asp23−Lys28 salt-bridge formation in Aβ10-35 monomers. J Am Chem Soc 128(50):16159–16168

80. Rodríguez MH, Morales LGF, Basurto JC, Hernández MCR (2018) Molecular docking and molecular dynamics simulation to evaluate compounds that avoid the amyloid beta 1–42 aggregation. In: Roy K (ed) Computational modeling of drugs against Alzheimer's disease. Springer, New York, pp 229–248

81. Amaro RE, Baudry J, Chodera J, Demir Ö, McCammon JA, Miao Y, Smith JC (2018) Ensemble docking in drug discovery. Biophys J 114(10):2271–2278

82. Cheng X, Ivanov I (2012) Molecular dynamic. Computat Toxicol I:243–285

83. Dong Y-w, Liao M-l, Meng X-l, Somero GN (2018) Structural flexibility and protein adaptation to temperature: molecular dynamics analysis of malate dehydrogenases of marine molluscs. Proc Natl Acad Sci 115(6):1274–1279

84. Gyebi GA, Ogunyemi OM, Ibrahim IM, Ogunro OB, Adegunloye AP, Afolabi SO (2021) SARS-CoV-2 host cell entry: an in silico investigation of potential inhibitory roles of terpenoids. J Genet Eng Biotechnol 1:91–22

85. Sinha S, Wang SM (2020) Classification of VUS and unclassified variants in BRCA1 BRCT repeats by molecular dynamics simulation. Comput Struct Biotechnol J 18:723–736

86. Daina A, Michielin O, Zoete V (2017) SwissADME: a free web tool to evaluate pharmacokinetics, drug-likeness and medicinal chemistry friendliness of small molecules. Sci Rep 7(1):42717

87. Veber DF, Johnson SR, Cheng H-Y, Smith BR, Ward KW, Kopple KD (2002) Molecular properties that influence the oral bioavailability of drug candidates. J Med Chem 45(12):2615–2623

88. Egan WJ, Merz KM, Baldwin JJ (2000) Prediction of drug absorption using multivariate statistics. J Med Chem 43(21):3867–3877

89. Ghose AK, Viswanadhan VN, Wendoloski JJ (1999) A knowledge-based approach in designing combinatorial or medicinal chemistry libraries for drug discovery. 1. A qualitative and quantitative characterization of known drug databases. J Comb Chem 1(1):55–68

90. Raschi E, Vasina V, Poluzzi E, De Ponti F (2008) The hERG K+ channel: target and antitarget strategies in drug development. Pharmacol Res 57(3):181–195

91. Kratz JM, Grienke U, Scheel O, Mann SA, Rollinger JM (2017) Natural products modulating the hERG channel: heartaches and hope. Nat Prod Rep 34(8):957–980

92. Mulliner D, Schmidt F, Stolte M, Spirkl H-P, Czich A, Amberg A (2016) Computational models for human and animal hepatotoxicity with a global application scope. Chem Res Toxicol 29(5):757–767

93. Wang N-N, Huang C, Dong J, Yao Z-J, Zhu M-F, Deng Z-K, Lv B, Lu A-P, Chen AF, Cao D-S (2017) Predicting human intestinal absorption with modified random forest approach: a comprehensive evaluation of molecular representation, unbalanced data, and applicability domain issues. RSC Adv 7(31):19007–19018

94. Xu Y, Dai Z, Chen F, Gao S, Pei J, Lai L (2015) Deep learning for drug-induced liver injury. J Chem Inf Model 55(10):2085–2093

95. Daina A, Zoete V (2016) A boiled-egg to predict gastrointestinal absorption and brain penetration of small molecules. ChemMedChem 11(11):1117–1121

96. Sapkota K, Mao Z, Synowicki P, Lieber D, Liu M, Ikezu T, Gautam V, Monaghan DT (2016) GluN2D N-methyl-d-aspartate receptor subunit contribution to the stimulation of brain activity and gamma oscillations

by ketamine: implications for schizophrenia. J Pharmacol Exp Ther 356(3):702–711

97. Pardridge WM (2009) Alzheimer's disease drug development and the problem of the blood-brain barrier. Alzheimers Dement 5(5):427–432

98. Van Wyk HM, Schoeman D, Kwembeya E, Hans RH, Pool EJ, Louw S (2022) In vitro acetylcholinesterase inhibitory activity and chemical composition of the dichloromethane extracts of the leaves and inflorescences of the tumbleweed, *Trachyandra laxa* (NE Br.) Oberm. Var. rigida (Suesseng.) Roessl. S Afr J Bot 147:231–237

99. Bosser A, Paplorey E, Belin J-M (1995) A simple way to (.+-.)-dihydroactinidiolide from. beta.-ionone related to the enzymic co-oxidation of. beta.-carotene in aqueous solution. Biotechnol Progress 11(6):689–692

100. Das M, Prakash S, Nayak C, Thangavel N, Singh SK, Manisankar P, Devi KP (2018) Dihydroactinidiolide, a natural product against Aβ25–35 induced toxicity in Neuro2a cells: synthesis, in silico and in vitro studies. Bioorg Chem 81:340–349

101. Oderfeld-Nowak B, Simon J, Chang L, Aprison M (1980) Interactions of the cholinergic and serotonergic systems: re-evaluation of conditions for inhibition of acetylcholinesterase by serotonin and evidence for a new inhibitor derived from this natural indoleamine. Gen Pharmacol Vasc Syst 11(1):37–45

102. Jin X, Wang M, Shentu J, Huang C, Bai Y, Pan H, Zhang D, Yuan Z, Zhang H, Xiao X (2020) Inhibition of acetylcholinesterase activity and β-amyloid oligomer formation by 6-bromotryptamine A, a multi-target anti-Alzheimer's molecule. Oncol Lett 19(2):1593–1601

103. Ghafary S, Ghobadian R, Mahdavi M, Nadri H, Moradi A, Akbarzadeh T, Najafi Z, Sharifzadeh M, Edraki N, Moghadam FH (2020) Design, synthesis, and evaluation of novel cinnamic acid-tryptamine hybrid for inhibition of acetylcholinesterase and butyrylcholinesterase. DARU J Pharm Sci 28:463–477

104. Ghafary S, Najafi Z, Mohammadi-Khanaposhtani M, Nadri H, Edraki N, Ayashi N, Larijani B, Amini M, Mahdavi M (2018) Novel cinnamic acid–tryptamine hybrids as potent butyrylcholinesterase inhibitors: synthesis, biological evaluation, and docking study. Arch Pharm 351(10):1800115

105. Wu J, Zhang H, Wang Y, Yin G, Li Q, Zhuo L, Chen H, Wang Z (2022) From tryptamine to the discovery of efficient multi-target directed ligands against cholinesterase-associated neurodegenerative disorders. Front Pharmacol 13:1036030

106. Jukic M, Politeo O, Maksimovic M, Milos M, Milos M (2007) In vitro acetylcholinesterase inhibitory properties of thymol, carvacrol and their derivatives thymoquinone and thymohydroquinone. Phytother Res 21(3):259–261. https://doi.org/10.1002/ptr.2063

107. Askin H, Yildiz M, Ayar A (2017) Effects of thymol and carvacrol on acetylcholinesterase from *Drosophila melanogaster*. Acta Phys Pol A 132(3):720–722

108. Bora RE, Bilgicli HG, Üç EM, Alagöz MA, Zengin M, Gulcin İ (2022) Synthesis, characterization, evaluation of metabolic enzyme inhibitors and in silico studies of thymol based 2-amino thiol and sulfonic acid compounds. Chem Biol Interact 366:110134

109. Silva SG, da Costa RA, de Oliveira MS, da Cruz JN, Figueiredo PLB, Brasil DSB, Nascimento LD, Chaves Neto AMJ, de Carvalho Junior RN, Andrade EHA (2019) Chemical profile of *Lippia thymoides*, evaluation of the acetylcholinesterase inhibitory activity of its essential oil, and molecular docking and molecular dynamics simulations. PLoS ONE 14(3):e0213393

Publisher's Note